Frontiers in Nanoscale Electrochemical Imaging: Faster, Multifunctional and Ultrasensitive

Minkyung Kang,[1] Dmitry Momotenko,[1] Ashley Page,[1,2] David Perry[1,2] and Patrick R. Unwin[1,]*

[1]Department of Chemistry and [2]MOAC Doctoral Training Centre, University of Warwick, Coventry, CV4 7AL, United Kingdom

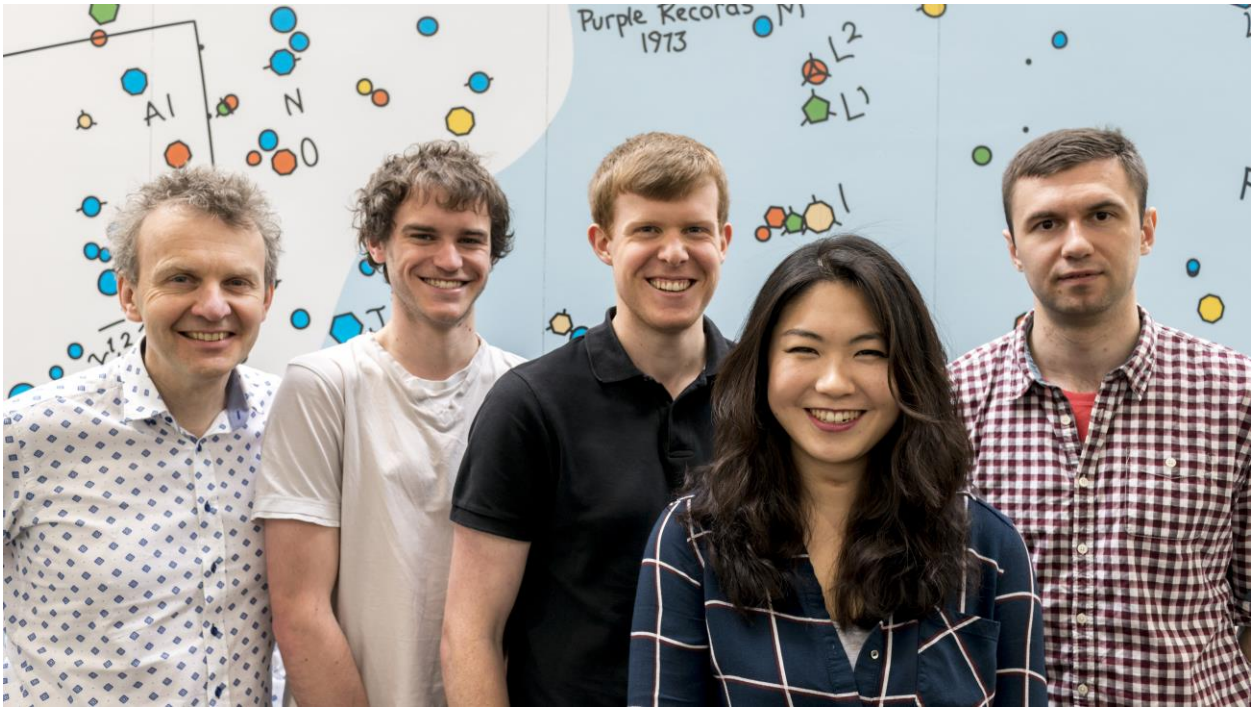

BIOGRAPHIES

Minkyung Kang is a Ph.D. candidate in Chemistry from the University of Warwick under the direction of Prof. Patrick Unwin. She received both her B.Sc. and M.Sc. in Chemistry from Ewha Womans University in South Korea where her research focused on applications of nano-structured metal oxides in electrochemical biosensors. Currently, she is studying the behavior of single entities (i.e. nanoparticles and molecules) at interfaces via electrochemical detection with scanning electrochemical cell microscopy.

Dmitry Momotenko graduated from M. V. Lomonosov Moscow State University, Russia in 2009 and received his Ph.D. at the École Polytechnique Fédérale de Lausanne, Switzerland in 2013, where he worked under supervision of Prof. Hubert Girault. Dmitry then received a Marie Curie Fellowship to work with Prof. Patrick Unwin at the University of Warwick, where his current research is focused on the development of electrochemical imaging techniques for probing surface reactivity and charge.

Ashley Page is a Ph.D. candidate under the supervision of Prof. Patrick Unwin in the Warwick Electrochemistry and Interfaces Group. He obtained a first class B.Sc. in Mathematics from the University of Warwick in 2013 before completing an M.Sc. in Mathematical Biology and Biophysical Chemistry at the MOAC Doctoral Training Centre the following year. His work focuses on the design and development of multi-channel electrochemical probes for the functional imaging of living cells.

David Perry attained a first class Master's degree in Mathematics from the University of Warwick in 2012 before undertaking a Master's degree in Mathematical Biology and

Biophysical Chemistry at the MOAC Doctoral Training Centre. Currently he is researching for a Ph.D. under the supervision of Prof. Patrick Unwin, exploring and developing the capabilities of the scanning ion conductance microscope for mapping cellular properties.

Patrick Unwin is a graduate of the universities of Liverpool (B.Sc., 1985), Oxford (D.Phil., 1989) and Warwick (D.Sc., 2008). He founded the Warwick Electrochemistry & Interfaces Group in 1992 and is presently Professor of Chemistry (since 1998) and Director of the Molecular Analytical Science Centre for Doctoral Training (since 2014). His interests are the development and application of flux imaging techniques and concepts, with wide applications including electrochemistry, cellular processes, materials characterization and crystal growth/dissolution.

ABSTRACT

A wide range of interfacial physicochemical processes, from electrochemistry to the functioning of living cells involve spatially localized chemical fluxes that are associated with specific features of the interface. Scanning electrochemical probe microscopes (SEPMs) represent a powerful means of visualizing interfacial fluxes, and this Feature Article highlights recent developments that have radically advanced the speed, spatial resolution, functionality and sensitivity of SEPMs. A major trend has been a coming together of SEPMs that developed independently, and the use of established SEPMs in completely new ways, greatly expanding their scope and impact. The focus is on nanopipette-based SEPMs, including scanning ion conductance microscopy (SICM), scanning electrochemical cell microscopy (SECCM), and hybrid techniques thereof, particularly with scanning electrochemical microscopy (SECM). Nanopipette-based probes are made easily, quickly and cheaply with tunable characteristics. They are reproducible and can be fully characterized, and their reponse can be modeled in considerable detail, so that quantitative maps of chemical fluxes and other properties (e.g. local charge) can be obtained and analyzed. This article provides an overview on the use of these probes for high speed imaging, to create movies of electrochemical processes in action, to carry out multifunctional mapping, such as simultaneous topography-charge and topography-activity, and to create nanoscale electrochemical cells for the detection, trapping and analysis of single entities, particularly individual molecules and nanoparticles (NPs). These studies provide a platform for the further application and diversification of SEPMs across a wide range of interfacial science.

1. Introduction

We are witnessing an incredible age of microscopy, where the structure and chemical properties of surfaces can be revealed and analyzed as never before on a wide range of length scales and in a diversity of environments. Many of these surfaces and the interfaces they form carry out functions that involve spatially-heterogeneous (non-uniform) chemical fluxes, yet our ability to map analyte concentrations and gradients near interfaces has lagged considerably behind structural microscopy. Recent developments in nanoscale electrochemical imaging highlighted in this Feature Article indicate that this situation is changing. New techniques are becoming available that have considerable capability for mapping and manipulating chemical fluxes near interfaces. The impact of these methods will be felt across a range of sciences, from materials characterization (e.g. understanding battery and fuel cell electrodes, and new catalyst discovery) to the life sciences (single cell analytics).

It is the purpose of this article to describe very recent developments in scanning electrochemical probe microscopy (SEPM) methods, both to illustrate what can be achieved now and, further, to signpost new directions for the future. There have been a number of recent reviews of SEPM methods, but the main focus of these has tended to be scanning electrochemical microscopy (SECM),[1] with ion conductance microscopy[2] and pipette-based methods also receiving some attention.[3] This article highlights, in particular, how SEPMs based on pipettes are especially promising. Nanopipettes are readily fabricated and characterized[4] to permit quantitative multifunctional analysis of a wide variety of surfaces and interfaces, with applications from cell biology[5] to materials characterization.[6] We analyze issues pertaining to the spatiotemporal response of SEPMs and describe recent advances that allow SEPMs to be

deployed on much faster timescales than ever before. This development leads to new prospects for creating *flux movies* of electrochemical and interfacial processes in action, providing an entirely new perspective and capability for analyzing interfaces. Finally, we show how new types of electrochemical nanocells can be created from novel SEPM tips containing multiple channels and sensors to facilitate studies of single entities, single nanoparticles (NPs) to individual molecules. This exciting field of study requires innovations in electrochemical instrumentation and methodology to measure very small signals (down to fA levels). We show that new SEPM probes are ideally suited for constructing nanoscale cells that can be used for counting, trapping and analyzing single NPs and single molecules that will serve to develop and grow this nascent field.

2. Prospects for Faster Electrochemical Imaging: Towards Quantitative Flux Movies

We begin by considering how SEPMs typically operate and how the rate of data acquisition, probe movement, and response could be speeded up to allow much quicker image acquisition, while also enhancing the spatial resolution. Achieving these aspirations would open up the possibility of recording detailed movies of electrochemical dynamics across an electrode (or other) surface, offering new views of electrochemical processes. This would be well beyond those attainable from both macroscopic voltammetry, which still dominates electrochemical measurements and necessarily averages over an entire electrode, and conventional SEPMs which provide a snapshot or handful of images (at best) of the distribution of activity across an electrode.

In a typical SEPM setup a probe electrode[1, 2] (or electrochemical cell)[7, 8] is brought within the vicinity of the surface or interface of interest and translated above the specimen at a constant height or at a constant probe-to-substrate distance, while recording the probe response (usually

current, but sometimes potential). The response is due to a specific type of interaction between the probe and the local environment at or near the sample, the nature of which depends on the electrochemical sensing technique and the application. Small scale microelectrode or nanoelectrode probes are employed for amperometric measurements in scanning electrochemical microscopy (SECM),[1] nanopipettes are utilized to probe local ion conductance and surface topography in scanning ion conductance microscopy (SICM),[2, 9] and double-barrel nanopipettes filled with electrolyte solution are used for the advanced scanning droplet cell platform, scanning electrochemical cell microscopy (SECCM).[7, 8] Hybrid techniques that combine the advantages of different scanning probe methods have also been developed, including combined SECM-SICM,[10, 11, 12] SECM-atomic force microscopy (AFM),[13, 14] or even more complex probe designs with extended functionality[15] as shown in Figure 1 which depicts an SECM probe (Figure 1a), an open nanopipette for SIC (Figure 1b), a double-barrel SECM-SICM hybrid probe with pyrolytic carbon nanoelectrode and an open barrel (Figure 1c), a double-barrel SECCM nanopipette (2 open channels, Figure 1d) and a quad-barrel probe, (two open barrels and two channels with deposited pyrolytic carbon (Figure 1e). These different probe designs have proven powerful for applications as diverse as the non-contact characterization of materials and material libraries,[16] energy systems analysis, interfacial processes and equilibria,[17] and for monitoring biointerfaces and living cells.[18, 19, 20, 21]

SEPMs tend to suffer from slow image acquisition rates. In a typical scanning experiment, data is recorded at frequencies that rarely exceed 1-10 pixels/s, which results in imaging times that usually range from tens of minutes to a few hours per image frame.[1] These low scanning dynamics are partly due to slow probe translation (usually only up to a few probe diameters per second at best), partly in order to avoid perturbation of mass-fluxes between the

probe and the substrate, but also due to the scan routines that have become embedded that use move, stop, measure protocols. These restrictions compromise the size of the scanned area, image quality (pixel density) and the number of image frames that can be acquired during an SEPM experiment. Long image exposure times also further impact the applicability of SEPMs due to associated problems, including thermal drift of piezoelectric positioners that control the tip and sample position, sample ageing, degradation/changes of chemical composition in the electrolytes, and probe contamination. Although the use of parallelized scanning techniques with multielectrode arrays of individually addressable electrodes[22, 23] overcomes some of these limitations, such approaches have not been used for the acquisition of multiple images with high frame rates.

In order to address and improve the slow image acquisition inherent in established SEPM techniques, consideration must be given to several important factors related to accurate probe translation/positioning, rapid data measurement/collection and high electrochemical probe response. First, faster probe scanning speeds during imaging requires piezoelectric positioning systems with high resonant frequencies. Typically, for a piezopositioner, equipped with an amplifier that can provide sufficient current output and slew rate, the time required for a full displacement is about a third of a period of the resonant frequency (but with a significant overshoot).[24] For example, for a piezoelectric stage with a 1 kHz resonant frequency, the displacement can occur within approximately 300 μs, but with relatively poor precision. In a closed-loop regime the capabilities of the servo controller and the sensor lag introduce additional delay in the displacement,[25] but significantly improve positioning accuracy and largely eliminate positioning hysteresis of piezoelectric components. Moreover, for full-range translation, the

dynamic performance of positioners can drop by one or two orders of magnitude,[25] and the dynamics are further affected by loading (cell, sample, tip etc.).

Typically in SEPM experiments, either a raster scan approach is taken,[26] whereby the probe is translated in a line-by-line rectangular pattern over the area of interest,[1] or a hopping mode is used whereby an image is constructed by approaching the SEPM probe to the sample at each image pixel.[27, 28] A few alternative harmonic movement trajectories, such as cycloid,[29] spiral[30, 31] and Lissajoux[32, 33] have been employed for better tracking in atomic force microscopy (AFM), but these strategies can also be used for almost any scanning probe technique to improve scan speeds. We discuss below the use of spiral scanning in SEPMs below and the considerable benefit that results.

The highest data collection rates that can be used with SEPMs are determined by the performance of the electronic components of potentiostats and current amplifiers, and IT issues (hardware and software). Typically, electrical current values in SEPMs vary between a few pA to a few nA (depending on the technique, probe size, species concentrations *etc.*), but in some cases can be as low as a few fA.[34] There is a well-known trade off between current amplification, bandwidth and noise[35] that must be taken into account in the design and use of current amplifiers, which places limitations on imaging speed and resolution (data acquisition rates) and precision (noise levels). High-speed electrochemical imaging requires amplifiers with high bandwidth, allowing full amplification of the signal within short timescales (1−10 μs) for the few pA to few nA range, with high-performance state of the art current followers).

Measured currents at SEPM probes are, further, the result of a convolution between the amplifier response and the electrochemical probe transient response time. For nanoscale probes, mass transport rates are particularly high, which makes them suitable for the task of high-speed

(steady-state) imaging: the diffusion time constant at a nanoscale disk electrode (employed in SECM) for example, is given by $\sim a^2/D$, and therefore is reasonably fast *e.g.* 2.5 μs for a probe with a radius, a, of 50 nm, assuming that a typical $D \sim 10^{-5}$ cm^2 s^{-1} for aqueous solution or organic solvent. In other SEPM imaging techniques (SECCM, SICM), mass transport rates can be enhanced if additional means of mass transport (*e.g.* migration in electric field) are introduced.[36]

Taking account of the aforementioned considerations, we have recently implemented high-speed imaging in SEPM setups, with frame rates approaching 4 s per image frame (3-4 orders of magnitude improvement over state of the art techniques). At this frame rate, images with 16500 pixels, at a pixel density of up to 1000 pixels μm^{-2} has been demonstrated using the SECCM platform (Figure 2a).[37] To achieve reliable positioning of nanoscale probes at high translation velocities (up to 100 μm s^{-1} with SECCM[37] and 180 μm s^{-1} with SICM[38] an Archimedes spiral scan pattern has been used (Figure 2b and c). Such a parametric scan trajectory allows for continuous probe movement (clockwise or counter-clockwise) from the spiral center outward for the forward scan and then back inward (reverse scan) toward the scan origin. In contrast to a raster scan pattern, the spiral scan trajectory is implemented to have a constant lateral speed and does not result in sharp changes of the translation direction. This smoother harmonic scan pattern (defined as sinusoids on each positioning axis with a 90 degree phase shift) prevents high accelerations (accompanied by high dynamic forces). This ensures precise probe positioning, without any compromise of the resulting image pixel density. In fact, as shown above and further herein, by acquiring data at a continuously moving probe, one achieves much better pixel spatial density than achieved in SECM hitherto.[1]

For imaging in a constant-distance mode, it is also important to consider the capabilities of the probe positional feedback. When vertical positioning relies on the ionic current through the nanopipette (SICM, SECCM),[2, 7, 8] modulation techniques with lock-in detection are often used to improve the signal-to-noise ratio[39] by measurement of the alternating current (AC) components.[40] The time constant of the AC modulation, defined as a few periods of the harmonic oscillation, is limited at the upper end by the resonant frequency of the piezoelectric positioner (if mechanical oscillation of the vertical probe position is used). The update rate of the positional feedback is therefore usually limited to frequencies around 1 kHz, or, equivalently, 1 ms intervals. With bias-modulation (BM-) techniques,[41] which do not involve physical oscillation of the probe position, the feedback can be employed at frequencies up to 30 kHz, enabling much faster response for high-speed applications. One can also employ a tracing protocol at slower translation rates, which permits the reliable acquisition of substrate topography, followed by a series of quick retrace scans at the desired (high) speed over a set of spatial coordinates (x, y and z), acquired in the trace step.[37] This approach can be implemented as long as precautions are taken to minimize drift of the piezoelectric positioners.[42]

The powerful capabilities of high-speed imaging with SECCM have been demonstrated[37] on several illustrative examples, including heterogeneous electron transfer rates on patterned self-assembled monolayers of thiol molecules on gold, electron transfer at an individual single walled carbon nanotube (SWNT) and surface-dispersed nanoscale electrocatalysts for water splitting. A particular advantage of high-speed electrochemical imaging is the possibility of acquiring hundreds of image frames while varying the experimental conditions, for example, the reaction driving potential.[37] This provides a huge volume of information on electrochemical activity that remains obscured when only a single image is recorded. This is of particular interest

for studying new materials, especially as these tend to have heterogeneous, and unusual, activity.[43]

Figure 3 demonstrates how this innovative strategy can be applied to an electrocatalytic system, comprising a highly-ordered pyrolytic graphite (HOPG) electrode decorated with iridium oxide (IrO_x) nanoparticles for the water splitting oxidation reaction (Figure 3a). The averaged current response across the entire image at low overpotentials suggests that both the substrate and the NP catalyst do not have significant activity, and the electrocatalytic effect of IrO_x particles becomes apparent only at relatively high reaction driving forces (above an applied potential of 0.8 V vs. Ag/AgCl QRCE, Figure 3b). However, the acquired images (see Figure 3c), reveals a striking difference between the activity of individual catalytic NPs. Moreover there is very high activity of some IrO_x particles even at significantly lower overpotential values than would be expected from the macroscopic observations.

It is important to point out that the high-speed imaging routine should be applicable to any electrochemical microscopy method. Indeed, high speed SICM for simultaneous topographical and reaction mapping are considered in section 2. SECCM, in fact, represents an example of a challenging SEPM for imaging at high dynamics, as it requires moving a liquid droplet over the substrate interface at high speed. Yet, it works well under these conditions. Other types of electrochemical microscopy usually operate under a relatively thick layer of electrolyte solution and therefore one has to consider a modified set of prerequisites for successful implementation of the high-speed imaging concept, mainly attributed to mass-transport of redox molecules and/or ions between the probe and the sample.

As discussed above, the time constant of the electrochemical probe is an important factor to be considered. For SECCM, the diffusional responses can be restrictive because diffusion is

limited by the conical pipette geometry.[37] However, the mass fluxes can be greatly enhanced, by a few orders of magnitude, when using ionic redox species, due to migration in the electric field, across the two channels of the nanopipette probe. On the other hand, the influence of convection (which can cause image blur in SEPMs such as, for instance, SECM)[44] is negligible, since it only acts on the liquid meniscus, whereas the concentration gradient typically extends some distance into the pipette.[36] When nanoscale probes are deployed, other SEPM techniques are also not expected to suffer from probe translation convective effects, since the fluid movement would be suppressed due to friction in the nanoscale probe-to-substrate gaps, and diffusive mass fluxes between the probe and surface would be rapid (see above).

An alternative way to create movies of electrochemical processes in action is to record a voltammogram at every pixel of an image. In this case, a move-stop-measure procedure is optimal. Data obtained can be replayed as a series of current maps as a function of potential or time, with the number of frames in the movie depending on the number of points in the voltammogram[45] or chronoamperogram[46] (for example). In typical practice, movies with many hundreds of frames are obtained which reveals important features and subtleties of interfacial electrochemical processes that are missed in conventional studies.

3. Multifunctional Electrochemical Imaging

The terms SECM and SICM were coined in the same year (1989),[9, 26] but the techniques developed along separate lines, with SECM receiving much more attention, diverse applications and, consequently, many more publications.[1] In contrast to SECM, SICM has been used predominantly for topographical imaging,[19, 47] with some work on local delivery from the SICM nanopipette probe[48, 49] and some studies considering the conductivity of porous membranes.[50] The ease with which probes with apertures as small as tens of nanometers can be fabricated and

fully characterized,[4] and the versatility of possible scan modes makes SICM a powerful technique for such applications, with resolutions comparable to AFM attainable.[51] Recent studies have shown that SICM can be extended beyond topographical imaging, and that simultaneous, topography-functional mapping is possible even with a single channel nanopipette, through clever adjustments of the SICM set up.[38, 52, 53, 54, 55] We illustrate this concept below for surface charge[52, 53, 54, 55] and surface activity[38] mapping. These new applications have come about through a much better understanding of the mass transport ion-flux processes and electric field effects that underpin the SICM response.[56] At the same time, the evident sensitivity of SICM to local heterogeneities in the ionic atmosphere of a substrate raises important questions about how best to employ SICM as a true topographical imaging technique, free from these phenomena – its original purpose. We discuss these issues below and show how SICM can be controlled to measure a range of surface properties of interest.

3.1 Bias Modulation SICM

It is important to first consider the principles of SICM and how the probe is positioned in the vicinity of a desired substrate. SICM uses the ionic current passing between two quasi-reference counter electrodes (QRCEs), one in the nanopipette probe and the other in the bulk electrolyte bath, to sense a surface. In conventional studies,[2, 19] a large voltage bias is applied between the two QRCEs and one of two feedback regimes is used: (i) the 'direct current' (DC) mode (Figure 4a), in which a drop in ionic current between the two electrodes is attributed to a close tip-substrate separation as a consequence of high gap resistance between the probe and surface, and (ii), the 'distance modulation' mode (DM, Figure 4b), which involves physically oscillating the pipette tip in the direction normal to the substrate surface with a sinusoidal motion of small amplitude, to induce an alternating current (AC) signal upon approach to the surface.[2] SICM is

increasingly popular tool for probing of soft interfaces such as living cells owing to the noncontact nature of these feedback methods.

We have recently developed an alternative mode of SICM feedback, whereby the physical oscillation of the nanopipette probe is replaced by a harmonic oscillation in the applied bias between the two QRCEs[57], as shown in Figure 4c. This bias modulated (BM) mode of feedback, as with DM-SICM, generates an AC signal that can be used for precise probe positioning near an interface. However, BM-SICM has several major advantages over more conventional SICM feedback modes that make it much more suitable for multi-functional SICM imaging. The key merit of BM-SICM is that it maintains sensitivity for topographical imaging, even when *no net bias* is applied, through the AC components of the ionic current recorded. The AC phase, detected with a lockin amplifier at the applied bias frequency, is sensitive to changes in the system resistance (tip-surface distance) and has been demonstrated to be at least as good as DM-SICM for topographical imaging,[41] with the further advantage that a much higher range of frequencies can be applied, opening up the prospect of faster scanning.

The SICM tip can be modeled well as a resistor and capacitor in parallel.[41] Upon approach of a tip to a sample, the system resistance increases and this results in a shift in the AC phase signal as more of the current flows more through the capacitative component of the system, resulting in an increase in a higher phase angle, as depicted in the example approach curve of Figure 4c. The benefits of this feedback mode will become apparent below, where SICM is discussed as a tool that can be used to unambiguously map both surface charge and topography in a new scanning regime.[53] Additional benefits of this feedback type include: (i) the removal of the physical oscillation of the tip, which could perturb the substrate (e.g. living cell); (ii) the elimination of significant electric fields at the end of the tip for topographic mapping,

which could otherwise significantly influence the substrate; (iii) the potential for closer tip-surface distances resulting the removal of the vertical tip oscillation, and consequently (iv) a wider range of accessible oscillation frequencies compared to the range that that can be applied to piezoelectric positioners.[41]

3.2 Simultaneous Surface Charge and Topographical Mapping with BM-SICM

To illustrate the possibility of SICM providing information on both the topography and other properties of an interface, with a single channel probe, we consider recent advances in charge mapping.[52, 53, 54, 55] Surface charge is important in a wide range of interfacial processes, and its importance in various functions of living cells is increasingly recognized,[58, 59] yet there are relatively few techniques for investigating charge density and heterogeneity on the nanoscale. SICM has the potential to fill this gap.

The use of SICM for the detection of interfacial charge is based on the ion current rectification phenomenon (ICR),[60] that is to say the nonlinear current-voltage response through a nanopipette (or nanopore) that arises when the thickness of the diffuse double layer (DDL) on the charged walls is no longer negligible compared to the opening size of the pipette. ICR is strongly influenced by both ionic strength and the geometry of a nanopipette, with the opening size and cone angle significantly affecting the magnitude of the observed effect.[61] Whereas in high concentration electrolytes (compressed DDL), there is generally a decrease in the ionic current when approaching a surface because of the increased gap resistance (Figure 4a), in lower electrolyte concentrations (extended DDL), the DDL influences the conductance at the end of the pipette, when near to the surface, changing the ICR behavior from that seen in bulk solution alone.[60] This surface induced rectification (SIR) phenomenon[52, 54] can be exploited to probe and map the charge of a substrate and is the basis of using SICM for surface charge mapping. On the

other hand, the sensitivity of the SICM response to surface charge, with an applied bias, suggests that surface charge effects and topographical features may be convoluted in conventional SICM formats (Figures 4a,b), particularly when very small tips are employed, even at relatively high ionic strength.

BM-SICM, neatly resolves the topography-surface charge issue.[53] FEM simulations have shown that the SICM AC response with no net bias renders the ionic current insensitive to surface charge effects, making it an accurate tool for topographical mapping.[53] As such, the following scan regime can be used: (i) the topography of the sample is extracted at zero net bias, using the difference in the AC phase between the bulk (Figure 5a) and the surface as a feedback signal; (ii) at each pixel in the topographical image, with the tip near the surface, surface charge is then elucidated by sweeping the bias between the two QRCEs (Figure 5b). This voltammetric response is then compared with a current-voltage (*I-V*) curve performed in bulk solution to reveal the effects of the substrate surface charge (Figure 5c).[53, 55] With this approach, the topography and charge of a surface can be investigated simultaneously and unambiguously. This highlights how SICM can become a powerful tool for multifunctional imaging by appropriate design of the potential control function.

This approach has been demonstrated for substrates that include polymer films and living cells. Figure 6 shows maps of an imperfect polystyrene film on glass,[53] imaged in 10 mM KCl solution. The SICM topography (a) reveals similar features as seen by AFM (b), but it can further be seen that both the DC (c, e) and the AC phase signals (d, f) are sensitive to variations in charge across the surface, when a potential bias is applied to the tip. At both positive and negative bias, the negative charge of the glass is clearly seen in contrast to the neutral polystyrene film.

In addition to experiments in low electrolyte concentrations, it has also been demonstrated that this technique can be used in physiologically relevant conditions (higher supporting electrolyte concentration) with living cells,[8] as shown in Figure 7. In this work, human adipocyte cells were imaged in the media in which they were grown, with an electrolyte concentration of around 150 mM. The negative surface charge of the section of the adipocyte cell imaged (Figure 7a,b) can be easily distinguished from the positively charged collagen substrate (used for cell attachment); see the SICM maps in Figure 7c, d, f and g. Significantly, surface charge heterogeneities on the cell membrane can be observed, in particular a feature along the length of the cell, which correlates with a topographical feature (Figure 7e). Given that this image was collected using a relatively large tip (diameter ~180 nm), these data demonstrate the sensitivity of the technique. The technique would become more sensitive to surface charge with smaller tips, while also improving the spatial resolution. These studies thus open up exciting prospects for the use of BM-SICM for identifying features on cell membranes through surface charge visualization, which could then be correlated to function. The technique is supported by a robust theoretical (FEM) model, which can be used to quantify the surface charge present at these interfaces, making it a quantitative and robust platform for multifunctional surface charge and topographical mapping. For the example shown in Figure 7, it was possible to determine a surface charge of 50 mC/m^2 for the collagen surface, in most areas of the cell the charge was -15 mC/m^2 and a positive charge of 50 mC/m^2 was found in the region along the center of the cell.

3.3 Electrochemical Reaction Mapping with SICM

SICM is also sensitive to changes in the local solution conductivity when an interfacial reaction occurs, and this can be sensed and used to visualize surface reaction rates. For example, the oxidation or reduction of an electroactive species at an electrode results in a change of ionic

composition near the electrode, and this can be sensed as a change in the ionic current through the nanopipette, opening up the possibility of using SICM for simultaneous topographical and reactivity mapping.[38]

This concept has been demonstrated for the hydrazine oxidation and proton reduction reaction at ~600 nm radius Pt UME, using a 200 nm-radius nanopipette (Figure 8a). These reactions result in a change in the solution composition (consumption of protons during reduction and release of H^+ for hydrazine oxidation) near the UME. Tuning of the tip potential provides a means of making the current response sensitive to either the topography or activity.[38] Moreover, for the example in Figure 8, and other cases, it is found that DM-SICM allowed probe positioning and topography mapping from the AC signal, even if there was a reaction at the interface, with the simultaneously recorded DC signal revealing the local activity. This therefore provides two approaches-DM-SICM and tuned bias SICM, to allow simultaneous topography-activity imaging with a single channel SICM tip. For the case in Figure 8, the probe approached the substrate at every image pixel (resulting in the detection of surface topography, Figure 8b) and a voltammogram (Figure 8c) was then recorded at the microelectrode substrate. The resulting changes in ionic conductance, detected by the nanopipette probe, could then be plotted as a sequence of image frames at different substrate potentials, providing movies of substrate reactivity. Figure 8d depicts 6 out of a total 380 images, showing the changes of ionic conductance at the UME due to proton reduction and hydrazine oxidation. The images demonstrate clear contrast between active (Pt) and inert (glass) areas on the sample.

High-speed variants of SICM have also recently been reported.[38, 62] Based on the principles outlined above, we have used SICM for high-speed multifunctional imaging, simultaneously mapping topography and electrochemical reactivity by monitoring conductance

changes in the vicinity of active reaction sites. For illustrative purposes, we considered the one-electron oxidation of ferrocenylmethyl trimethylammonium hexafluorophosphate, $FcTMA^+$, at a small UME substrate.[38] The oxidation of $FcTMA^+$ to $FcTMA^{2+}$ causes an influx of electrolyte anions and efflux of electrolyte cations near the electrode to maintain electroneutrality that results in a changed ionic composition. Figure 9b, is a slower trace prescan at the active substrate, which clearly shows the site of the reaction to be highlighted with a lower pipette tip current over the Pt UME. Faster scanning then allowed the effects of varying substrate potential to be elucidated through high speed scans with different applied substrate potentials. The probe was translated at a rate 35 times faster than during the prescan and it was confirmed there was little influence of the probe translation speed on the image quality and measured probe responses, as seen in Figure 9c. Six images from 101 recorded are shown in Figure 9d, at a series of decreasing substrate potentials that gradually switches off the reaction. This example further illustrates the power of high-speed functional imaging. One attains a similar potential resolution as voltammetry, but rather than measuring the *average response*, the activity is viewed as a current map of the surface, in this case of >16,000 pixels.

3.4 Multi-channel Probes for Multifunctional Imaging

While single channel SICM is powerful for multifunctional imaging, hybrid techniques such as SECM-AFM[63] and SECM-SICM[10, 11] diversify the scope and applications of functional and electrochemical imaging. In the case of SECM-SICM, the simplest probe design uses a theta pipette, where one open channel is filled with electrolyte and a QRCE for SICM measurements and the other filled with pyrolytic carbon for SECM detection[11] although an alternative design is possible.[10, 12] The SICM barrel can be used to independently position the nanopipette probe near a substrate of interest, while the SECM probe can further measure an analyte of interest, for

example pH,[17] or other ions/molecules by electrolysis.[11] For pH sensing, the carbon electrode is coated with iridium oxide allowing potentiometric pH measurements to be undertaken.[17] Functionalization of the carbon electrode with platinum also permits measurements of O_2[64, 65] and H_2O_2[66] by amperometry.

SEPMs, and specifically nanopipette-based electrochemical techniques, are not limited to two channels. Quad-barrel (four channel) probes with two solid carbon channels and two channels filled with electrolyte solution have been fabricated to extend further the functionality of nanopipette-based techniques.[15] Deploying this quad-barrel probe in a SECCM regime creates a highly localized electrochemical cell that can be used for sensing analytes or driving/detecting electrochemical reactions concurrently whilst still allowing accurate topographical imaging through the SECCM feedback between the open barrels.[15] Thus far, these probes have been shown to be capable of performing generator-collection experiments at individual SWNTs, as well as some other applications considered below. These multi-channel probes could find great application in the study of living cells, for example, where the cell membrane could be stimulated through one pipette barrel, or material delivered, whilst detecting the cellular response in several others, an approach that would essentially produce a lab-on-a-tip.[7] An attraction of pipette-based probes for local analysis is that they can perform nanobiopsies on cells,[67] and one could imagine building in new functions quite easily, such as tip-enhanced Raman spectroscopy. Field effect transistor (FET) devices based on dual carbon nanoelectrodes[17] have recently been reported,[68] and these could usefully be developed on a multichannel device to enable topography-activity imaging.

4. Ultrasensitive measurements

4.1 Mapping the Electrochemical Activity of Single Entities

Nanomaterials (metal nanoparticles, carbon nanotubes, *etc.*) are rather heterogeneous, and small variations of the shape, size, structure, reactive sites and surface defects can have a dramatic effect on activity. Gaining access to such information at a single entity (*e.g.* single particle), or even at a sub-single entity level is therefore vital to understanding how these materials work, although it is experimentally challenging.

SECM, as the most widely used SEPM hitherto, has been employed extensively to study electrochemical kinetics,[69] and has been applied to investigate heterogeneous processes in a nanogap configuration[70, 71] and for electrochemical imaging and kinetic studies of single NPs.[72] However, special attention must be paid to several factors for the application of SECM at the nanoscale, particularly adsorption effects,[71] and the difficulty of maintaining, and knowing the probe-to-substrate separation where there is no positional feedback during imaging:[72] even small changes in working distance, caused by sample tilt, topographical features and the effects of thermal drift of piezoelectric positioners,[42] as well as non-ideal tip geometry, could cause serious misinterpretation of experimental data. In contrast, the combined SECM-SICM approach, with independent control of probe positioning can be used to study the electrocatalytic properties of single NPs, resulting in high-resolution maps of topography and electrochemistry, as exemplified by the visualization of hydrogen peroxide production at Au NPs.[66]

The SECCM configuration offers a different way of confining an electrochemical measurement to a smaller area (footprint), via contact from a liquid meniscus at the tip of the double-barrel SECCM pipette, with a contact diameter of as small as 90 nm attainable.[43] The small contact area of SECCM leads to low background currents and relatively low capacitance (during potential scanning or transient phenomena), as well as allowing the study of the most diverse range of substrate electrodes. SECCM has been utilized successfully to visualize the

electrocatalytic activity of single platinum NPs deposited on a SWNT for the oxygen reduction reaction (ORR) and hydrogen evolution reaction (HER)).[73] It was possible to analyze the ORR response at tens of fA at relatively low overpotentials (0.5 V, Figure 10a) up to the pA current range at more cathodic substrate potentials. This study highlighted the considerable value of correlative microscopic analysis, with AFM and FE-SEM allowing access to individual particle size, shape and reactivity (Figure 10b and c). In similar fashion, SECCM has been used to pinpoint the active sites for electrochemistry at SWNTs,[74, 75] showing, for example, that kinks in SWNTs facilitate the electro reduction of O_2 to H_2O_2[75] and enabling electrochemical kinetics to be related to the size and electrical properties of SWNTs.[74]

4.2 Nanoparticle Impact Studies

The SECCM platform, with a static probe, presents a very attractive configuration for the delivery of NPs to a substrate surface and for probing the dynamics and catalytic properties through the analysis of NP collisions. This is an alternative approach to the typical ultramicroelectrode (UME)-based measurements,[76, 77, 78] that are employed for such studies. SECCM offers: (i) a much wider range of substrate electrodes, because there is no need for encapsulation of the substrate electrode material as a UME; (ii) much smaller electrode size and (iii) as a consequence, greatly diminished background currents, far superior to those attainable in other formats. Furthermore, as we outline below, careful design of the current amplification system allows both the more complete analysis of transient events and detection of short-lived phenomena that are missed by other studies.[79, 80]

The key features of the SECCM setup for single NP impact measurements are shown in Figure 11a. This simple schematic highlights important aspects of an electrochemical cell that

forms meniscus contact with a substrate electrode: there is a wide choice of possible substrate electrodes, ensuring that background current signals are much lower than with UMEs. The fact that the positionable droplet cell can be applied over almost any (semi-) conductive surface of interest allows the interaction of NPs with a broad range of materials to be studied, whereas the range of materials for UME fabrication is rather limited. Furthermore, the QRCEs in the pipette create an electric field that can be used to deliver particles to a surface[81] and the current response could be used to count particles (resistive pulse).[82]

We have recently studied the impact of Au NPs on Au surfaces functionalized with self-assembled monolayers of alkane thiols with different terminal groups, exploring how the surface chemistry influences the residence time and electron transfer (ET) kinetics, as manifest in the outer sphere oxidation of $Fe(CN)_6^{4-}$ to $Fe(CN)_6^{3-}$ (Figure 11b). Surface chemistry effects in impact measurements have rarely been explored, and these studies revealed strong surface chemistry effects.[80] When a NP resides only transiently on a substrate electrode (and for other transient phenomena in NP impact studies), it is important to consider how the bandwidth of the current amplifier in relation to the residence time of the NP on the substrate surface influences the transient signal recorded. This important aspect of NP impact studies has been somewhat overlooked, although it has been considered in single molecule electrochemical detection.[83] Where the occupancy of NPs on a substrate is shorter than the time constant of the current amplifier a greatly attenuated electrochemical response is observed.[80] This point is illustrated in Figure 11c, which shows the convolution of the current response arising from a diffusion-limited NP reaction (e.g. $Fe(CN)_6^{4+}$ for different NP occupancy times for a current follower with a bandwidth of 20 ms.

NP impact studies with high bandwidth SECCM have revealed considerable insight into NP transport and interactions with an electrode surface.[79] Three-dimensional random walk simulations of single NPs in the SECCM meniscus were used to aid understanding of the NP dynamics and current response observed.[79] A hydrodynamic trapping model was used, whereby the NP displays hindered diffusion near to the substrate electrode surface. A computed trajectory of a NP and its occupancy on a substrate surface is shown in Figure 12a, along with averaged occupancy on the electrode, as would manifest in experimental *i-t* traces convoluted by the current amplifier response (bandwidth 10 μs).

Studies of the electro-oxidation of H_2O_2 at RuO_x NPs enabled the detection of NPs with a finite arrival time due to the NP hindered diffusion coefficient, for which experiments and simulations were modeled (Figure 12b). However, while the hydrodynamic trapping model predicted a NP to remain near the substrate electrode, experimental measurements showed that NPs tended to leave the electrode surface. We have attributed this as being due to electrochemical propulsion from O_2 gas evolution, as a result of H_2O_2 oxidation.[84] After leaving the electrode, this reaction switches off and NPs drift back into contact with the electrode. This leads to a repetitive trapping-and-release process that has not been recognized previously. As a consequence, impact frequencies are several orders of magnitude higher than expected based on a single pass diffusive model that has mainly been used to analyze impact frequencies in NP impact studies.[85]

Under certain conditions, NPs adhere to electrodes after impact. With SECCM this opens up the possibility of correlating NP electrochemistry with structure by using a transmission electron microscopy (TEM) grid as the substrate,[86] so that high resolution TEM characterization of a NP can be carried out after electrochemical measurement.

4.3 Single Molecule Electrochemical Detection (SMED)

SMED is perhaps the ultimate measurement in elecroanalytical chemistry and extremely challenging due to the small current signals involved. Micro- and nanoelectrodes have been used to monitor catalytic responses from a single enzyme[87] or a few enzyme molecules.[88] Due to their low background noise levels, field effect transistor (FET) devices have also been sensitive tools for single molecule applications, where the detection principle is typically based on the change in conductance at a certain voltage threshold due to the charge transfer from an analyte molecule.[89, 90]

An alternative configuration for SMED is based on the confinement of the electrochemical measurement in a very small volume between two closely spaced, opposing electrodes, so that the electrochemical current can be significantly amplified by redox cycling of a trapped molecule.[91] In such a configuration, the redox species works as an electron shuttle that bounces between a cathode and an anode at high frequency. The amplification and sensitivity of these devices are dependent on the mass-transport rate (which is determined mainly by, d, the interelectrode distance, with the diffusion time $\propto d^{-2}$). While electrochemical cells with nanogaps can be fabricated lithographically,[83] there are limitations as to the electrode materials and gap sizes that can be used.

We recently reported SMED using quad-barrel probes in an SECCM configuration[34] Reproducibility of probe fabrication was achieved by milling the probe end with a focused ion beam (FIB), resulting in two electrodes that could provide redox cycling with the substrate electrode and two open channels filled with a dilute electrolyte solution of a redox species (10 – 100 nM) that maintained a stable meniscus at the end of the pipette (Figure 1e). The quad-probe

was approached to the substrate until the meniscus came into contact with the substrate electrode, producing a nanogap cell to carry out single molecule redox cycling. Anticorrelated currents with a magnitude of a few fA were observed within the tens of nanometers gap between the tip and the substrate electrodes, corresponding to SMED with a current magnitude similar to that predicted by random walk simulations. This droplet (meniscus contact) regime resulted in extremely low background noise allowing the application of SMED in new environments, such as ionic liquids where the diffusion coefficient is much lower than in an aqueous system. The use of a quad-barrel probe in an SECCM configuration opens up further applications to various single entity measurements, including SMED. For example, since these probes contain channels for delivery/extraction with electric field control and electrochemical sensing, one could envisage adaptive experiments where control-detection functions were built into this type of cell for the manipulation, characterization and analysis of single entities.

5. Conclusions and Outlook

Although SEPMs, for example SECM and SICM have been in existence for more than a quarter of a century, this family of techniques is at an exciting nexus where the mixing of SECM and SICM principles, and probes, is leading to major new developments that allow interfacial flux processes to be mapped quantitatively at the nanoscale in unprecedented detail. Coupled with these advances, there has been substantial recent progress in SEPM instrumentation, such that probes can be moved over a surface and acquire data orders of magnitude faster than previously, with data acquisition rates close to MHz now realizable. These developments open up new vistas on electrochemical interfacial processes, by allowing, for example, the recording of movies of electrochemical fluxes as a function of potential or time, which reveal new aspects to the influence of electrode structure on activity. In the future, these high bandwidth capabilities will

also be of considerable benefit for large area scanning, patterning and combinatorial electrochemistry, for example, in catalyst screening studies.

A long-standing problem in SEPM has been the separation of topography and interfacial activity. The power of SECM is in mapping reactive fluxes, but the response is highly sensitive to the probe to substrate separation, which is difficult to determine in the conventional, and widely used, SECM configuration. On the other hand, SICM developed purely as a topographical imaging tool, or a means of local delivery and stimulation. Very recent progress, highlighted in this article, has shown that by re-analyzing and re-casting SICM as an electrochemical technique, it is possible to better understand the response through which SICM can be used to map functional properties such as interfacial charge or reactivity, alongside topography, with a simple single channel nanopipette. Furthermore, dual SECM-SICM nanoprobes that are easy to make and characterize bring together the considerable capabilities of the two techniques for functional imaging.

Topography and activity are also readily separated in SECCM, the most sophisticated scanning droplet technique available, where a dual channel probe containing electrolyte and a QRCE in each channel can be used for highly sensitive localized electrochemical measurements. This technique is particularly powerful when combined with other microscopy techniques applied to the same area of a material. We have shown how SECCM can reveal a wealth of information on the electrochemical properties of nanomaterials and also to deliver nanomaterials to a surface, as exemplified by NP impact studies, where SECCM offers a platform with considerably lower background currents, so that the electrochemical response for NP impacts can be analyzed in much more detail than in alternative configurations. There are prospects for further enhancing this platform, for example, using the resistive pulse when a NP is delivered to

a substrate to measure the size of a NP as it impinges on an electrode, and using the electric field across the end of the SECCM tip and meniscus to control, move and trap NPs in the meniscus.

We have also highlighted emerging studies that use up to four channels in a small footprint probe. This constitutes the beginning of a lab-on-a-tip that will allow a multitude of future applications, such as more sophisticated sensors based on FETs, nanoscale titrations, charge mapping-uptake studies and many other uses. It should also be possible to introduce complementary spectroscopic and nanoscopic sampling capability into this type of probe, turning it into a nano-tool of great flexibility.

References

1. Bard, A. J.; Mirkin, M. V. *Scanning electrochemical microscopy*; CRC Press2012.
2. Chen, C. C.; Zhou, Y.; Baker, L. A. Scanning ion conductance microscopy. *Annu. Rev. Anal. Chem.* **2012,** *5*, 207-28.
3. Kranz, C. Recent advancements in nanoelectrodes and nanopipettes used in combined scanning electrochemical microscopy techniques. *Analyst* **2014,** *139* (2), 336-352.
4. Perry, D.; Momotenko, D.; Lazenby, R. A.; Kang, M.; Unwin, P. R. Characterization of Nanopipettes. *Anal. Chem.* **2016,** *88* (10), 5523–5530.
5. Klenerman, D.; Korchev, Y. E.; Davis, S. J. Imaging and characterisation of the surface of live cells. *Curr. Opin. Chem. Biol.* **2011,** *15* (5), 696-703.
6. Barton, Z. J.; Rodríguez-López, J. Emerging scanning probe approaches to the measurement of ionic reactivity at energy storage materials. *Anal. Bioanal. Chem.* **2016,** *408* (11), 2707-2715.
7. Aaronson, B. D. B.; Güell, A. G.; McKelvey, K.; Momotenko, D.; Unwin, P. R. Scanning Electrochemical Cell Microscopy: Mapping, Measuring, and Modifying Surfaces and Interfaces at the Nanoscale. In *Nanoelectrochemistry*; CRC Press, 2015, pp 655-694.
8. Ebejer, N.; Güell, A. G.; Lai, S. C. S.; McKelvey, K.; Snowden, M. E.; Unwin, P. R. Scanning Electrochemical Cell Microscopy: A Versatile Technique for Nanoscale Electrochemistry and Functional Imaging. *Annu. Rev. Anal. Chem.* **2013,** *6* (1), 329-351.
9. Hansma, P. K.; Drake, B.; Marti, O.; Gould, S. A.; Prater, C. B. The Scanning Ion-Conductance Microscope. *Science* **1989,** *243* (4891), 641-3.
10. Takahashi, Y.; Shevchuk, A. I.; Novak, P.; Murakami, Y.; Shiku, H.; Korchev, Y. E.; Matsue, T. Simultaneous Noncontact Topography and Electrochemical Imaging by SECM/SICM Featuring Ion Current Feedback Regulation. *J. Am. Chem. Soc.* **2010,** *132* (29), 10118-10126.
11. Takahashi, Y.; Shevchuk, A. I.; Novak, P.; Zhang, Y. J.; Ebejer, N.; Macpherson, J. V.; Unwin, P. R.; Pollard, A. J.; Roy, D.; Clifford, C. A.; Shiku, H.; Matsue, T.; Klenerman, D.; Korchev, Y. E. Multifunctional Nanoprobes for Nanoscale Chemical Imaging and Localized Chemical Delivery at Surfaces and Interfaces. *Angew. Chem. Int. Edit.* **2011,** *50* (41), 9638-9642.
12. Comstock, D. J.; Elam, J. W.; Pellin, M. J.; Hersam, M. C. Integrated Ultramicroelectrode-Nanopipet Probe for Concurrent Scanning Electrochemical Microscopy and Scanning Ion Conductance Microscopy. *Anal. Chem.* **2010,** *82* (4), 1270-1276.
13. Macpherson, J. V.; Unwin, P. R. Combined scanning electrochemical-atomic force microscopy. *Anal. Chem.* **2000,** *72* (2), 276-285.
14. Kranz, C.; Friedbacher, G.; Mizaikofft, B.; Lugstein, A.; Smoliner, J.; Bertagnolli, E. Integrating an ultramicroelectrode in an AFM cantilever: Combined technology for enhanced information. *Anal. Chem.* **2001,** *73* (11), 2491-2500.
15. Nadappuram, B. P.; McKelvey, K.; Byers, J. C.; Güell, A. G.; Colburn, A. W.; Lazenby, R. A.; Unwin, P. R. Quad-Barrel Multifunctional Electrochemical and Ion Conductance Probe for Voltammetric Analysis and Imaging. *Anal. Chem.* **2015,** *87* (7), 3566-3573.
16. Fernandez, J. L.; Walsh, D. A.; Bard, A. J. Thermodynamic guidelines for the design of bimetallic catalysts for oxygen electroreduction and rapid screening by scanning electrochemical microscopy. M-Co (M: Pd, Ag, Au). *J. Am. Chem. Soc.* **2005,** *127* (1), 357-365.
17. Nadappuram, B. P.; McKelvey, K.; Al Botros, R.; Colburn, A. W.; Unwin, P. R. Fabrication and characterization of dual function nanoscale pH-scanning ion conductance

microscopy (SICM) probes for high resolution pH mapping. *Anal. Chem.* **2013,** *85* (17), 8070-8074.
18. Lin, T.-E.; Bondarenko, A.; Lesch, A.; Pick, H.; Cortés-Salazar, F.; Girault, H. H. Monitoring Tyrosinase Expression in Non-metastatic and Metastatic Melanoma Tissues by Scanning Electrochemical Microscopy. *Angew. Chem. Int. Edit.* **2016,** *55* (11), 3813-3816.
19. Korchev, Y. E.; Bashford, C. L.; Milovanovic, M.; Vodyanoy, I.; Lab, M. J. Scanning ion conductance microscopy of living cells. *Biophys. J.* **1997,** *73* (2), 653-658.
20. Shevchuk, A. I.; Frolenkov, G. I.; Sanchez, D.; James, P. S.; Freedman, N.; Lab, M. J.; Jones, R.; Klenerman, D.; Korchev, Y. E. Imaging Proteins in Membranes of Living Cells by High-Resolution Scanning Ion Conductance Microscopy. *Angew. Chem. Int. Edit.* **2006,** *45* (14), 2212-6.
21. Lee, C. M.; Kwak, J. Y.; Bard, A. J. Application of Scanning Electrochemical Microscopy to Biological Samples. *Proc. Natl. Acad. Sci. USA* **1990,** *87* (5), 1740-1743.
22. Cortes-Salazar, F.; Momotenko, D.; Lesch, A.; Wittstock, G.; Girault, H. H. Soft Microelectrode Linear Array for Scanning Electrochemical Microscopy. *Anal. Chem.* **2010,** *82* (24), 10037-10044.
23. Barker, A. L.; Unwin, P. R.; Gardner, J. W.; Rieley, H. A Multi-Electrode Probe for Parallel Imaging in Scanning Electrochemical Microscopy. *Electrochem. Commun.* **2004,** *6* (1), 91-97.
24. PI. http://www.piceramic.com/piezo-technology/properties-piezo-actuators/dynamic-operation.html (accessed 13th May 2016).
25. Fleming, A. J.; Leang, K. K. *Design, Modeling and Control of Nanopositioning Systems*; Springer: Cham, 2014. p 411.
26. Kwak, J.; Bard, A. J. Scanning electrochemical microscopy. Apparatus and two-dimensional scans of conductive and insulating substrates. *Anal. Chem.* **1989,** *61* (17), 1794-1799.
27. Novak, P.; Li, C.; Shevchuk, A. I.; Stepanyan, R.; Caldwell, M.; Hughes, S.; Smart, T. G.; Gorelik, J.; Ostanin, V. P.; Lab, M. J. Nanoscale live-cell imaging using hopping probe ion conductance microscopy. *Nat. Methods* **2009,** *6* (4), 279-281.
28. Borgwarth, K.; Ebling, D.; Heinze, J. Scanning electrochemical microscopy: a new scanning mode based on convective effects. *Ber. Bunsenges. Phys. Chem* **1994,** *98* (10), 1317-1321.
29. Yong, Y. K.; Moheimani, S. O.; Petersen, I. R. High-Speed Cycloid-Scan Atomic Force Microscopy. *Nanotechnology* **2010,** *21* (36), 365503.
30. Ziegler, D.; Meyer, T. R.; Farnham, R.; Brune, C.; Bertozzi, A. L.; Ashby, P. D. Improved Accuracy and Speed in Scanning Probe Microscopy by Image Reconstruction from Non-Gridded Position Sensor Data. *Nanotechnology* **2013,** *24* (33), 335703.
31. Mahmood, I. A.; Moheimani, S. O. Fast Spiral-Scan Atomic Force Microscopy. *Nanotechnology* **2009,** *20* (36), 365503.
32. Tuma, T.; Lygeros, J.; Kartik, V.; Sebastian, A.; Pantazi, A. High-Speed Multiresolution Scanning Probe Microscopy Based on Lissajous Scan Trajectories. *Nanotechnology* **2012,** *23* (18), 185501.
33. Yong, Y. K.; Bazaei, A.; Moheimani, S. O. R.; Allgower, F. In *Design and Control of a Novel Non-Raster Scan Pattern for Fast Scanning Probe Microscopy*, Advanced Intelligent Mechatronics (AIM), 2012 IEEE/ASME International Conference on, 11-14 July 2012; 2012, pp 456-461.

34. Byers, J. C.; Paulose Nadappuram, B.; Perry, D.; McKelvey, K.; Colburn, A. W.; Unwin, P. R. Single molecule electrochemical detection in aqueous solutions and ionic liquids. *Anal. Chem.* **2015,** *87* (20), 10450-10456.
35. Carminati, M.; Ferrari, G.; Bianchi, D.; Sampietro, M. Femtoampere integrated current preamplifier for low noise and wide bandwidth electrochemistry with nanoelectrodes. *Electrochim. Acta* **2013,** *112*, 950-956.
36. Snowden, M. E.; Güell, A. G.; Lai, S. C.; McKelvey, K.; Ebejer, N.; O'Connell, M. A.; Colburn, A. W.; Unwin, P. R. Scanning electrochemical cell microscopy: Theory and experiment for quantitative high resolution spatially-resolved voltammetry and simultaneous ion-conductance measurements. *Anal. Chem.* **2012,** *84* (5), 2483-2491.
37. Momotenko, D.; Byers, J. C.; McKelvey, K.; Kang, M.; Unwin, P. R. High-Speed Electrochemical Imaging. *ACS Nano* **2015,** *9* (9), 8942-8952.
38. Momotenko, D.; McKelvey, K.; Kang, M.; Meloni, G. N.; Unwin, P. R. Simultaneous Interfacial Reactivity and Topography Mapping with Scanning Ion Conductance Microscopy (SICM). *Anal. Chem.* **2016**.
39. Voigtländer, B. Lock-In Technique. In *Scanning Probe Microscopy: Atomic Force Microscopy and Scanning Tunneling Microscopy*; Springer Berlin Heidelberg: Berlin, Heidelberg, 2015, pp 101-105.
40. Shevchuk, A. I.; Gorelik, J.; Harding, S. E.; Lab, M. J.; Klenerman, D.; Korchev, Y. E. Simultaneous measurement of Ca2+ and cellular dynamics: combined scanning ion conductance and optical microscopy to study contracting cardiac myocytes. *Biophys. J.* **2001,** *81* (3), 1759-1764.
41. McKelvey, K.; Perry, D.; Byers, J. C.; Colburn, A. W.; Unwin, P. R. Bias Modulated Scanning Ion Conductance Microscopy. *Anal. Chem.* **2014,** *86* (7), 3639-3646.
42. Kim, J.; Shen, M.; Nioradze, N.; Amemiya, S. Stabilizing nanometer scale tip-to-substrate gaps in scanning electrochemical microscopy using an isothermal chamber for thermal drift suppression. *Anal. Chem.* **2012,** *84* (8), 3489-3492.
43. Güell, A. G.; Cuharuc, A. S.; Kim, Y.-R.; Zhang, G.; Tan, S.-y.; Ebejer, N.; Unwin, P. R. Redox-dependent spatially resolved electrochemistry at graphene and graphite step edges. *ACS Nano* **2015,** *9* (4), 3558-3571.
44. Combellas, C.; Fermigier, M.; Fuchs, A.; Kanoufi, F. Scanning electrochemical microscopy. Hydrodynamics generated by the motion of a scanning tip and its consequences on the tip current. *Anal. Chem.* **2005,** *77* (24), 7966-7975.
45. Chen, C.-H.; Jacobse, L.; McKelvey, K.; Lai, S. C.; Koper, M. T.; Unwin, P. R. Voltammetric scanning electrochemical cell microscopy: dynamic imaging of hydrazine electro-oxidation on platinum electrodes. *Anal. Chem.* **2015,** *87* (11), 5782-5789.
46. Takahashi, Y.; Kumatani, A.; Munakata, H.; Inomata, H.; Ito, K.; Ino, K.; Shiku, H.; Unwin, P. R.; Korchev, Y. E.; Kanamura, K. Nanoscale visualization of redox activity at lithium-ion battery cathodes. *Nat. Commun.* **2014,** *5* (5540), 7.
47. Takahashi, Y.; Murakami, Y.; Nagamine, K.; Shiku, H.; Aoyagi, S.; Yasukawa, T.; Kanzaki, M.; Matsue, T. Topographic imaging of convoluted surface of live cells by scanning ion conductance microscopy in a standing approach mode. *Phys. Chem. Chem. Phys.* **2010,** *12* (34), 10012-10017.
48. Ying, L.; Bruckbauer, A.; Rothery, A. M.; Korchev, Y. E.; Klenerman, D. Programmable delivery of DNA through a nanopipet. *Anal. Chem.* **2002,** *74* (6), 1380-1385.

49. Bruckbauer, A.; James, P.; Zhou, D.; Yoon, J. W.; Excell, D.; Korchev, Y.; Jones, R.; Klenerman, D. Nanopipette delivery of individual molecules to cellular compartments for single-molecule fluorescence tracking. *Biophys. J.* **2007,** *93* (9), 3120-3131.
50. Chen, C.-C.; Derylo, M. A.; Baker, L. A. Measurement of ion currents through porous membranes with scanning ion conductance microscopy. *Anal. Chem.* **2009,** *81* (12), 4742-4751.
51. Rheinlaender, J.; Geisse, N. A.; Proksch, R.; Schäffer, T. E. Comparison of scanning ion conductance microscopy with atomic force microscopy for cell imaging. *Langmuir* **2010,** *27* (2), 697-704.
52. Sa, N.; Lan, W.-J.; Shi, W.; Baker, L. A. Rectification of Ion Current in Nanopipettes by External Substrates. *ACS Nano* **2013,** *7* (12), 11272-11282.
53. Perry, D.; Al Botros, R.; Momotenko, D.; Kinnear, S. L.; Unwin, P. R. Simultaneous Nanoscale Surface Charge and Topographical Mapping. *ACS Nano* **2015,** *9* (7), 7266-76.
54. McKelvey, K.; Kinnear, S. L.; Perry, D.; Momotenko, D.; Unwin, P. R. Surface Charge Mapping with a Nanopipette. *J. Am. Chem. Soc.* **2014,** *136* (39), 13735-13744.
55. Perry, D.; Paulose Nadappuram, B.; Momotenko, D.; Voyias, P. D.; Page, A.; Tripathi, G.; Frenguelli, B. G.; Unwin, P. R. Surface Charge Visualization at Viable Living Cells. *J. Am. Chem. Soc.* **2016**.
56. Edwards, M. A.; Williams, C. G.; Whitworth, A. L.; Unwin, P. R. Scanning ion conductance microscopy: a model for experimentally realistic conditions and image interpretation. *Anal. Chem.* **2009,** *81* (11), 4482-4492.
57. McKelvey, K.; Perry, D.; Byers, J. C.; Colburn, A. W.; Unwin, P. R. Bias modulated scanning ion conductance microscopy. *Anal. Chem.* **2014,** *86* (7), 3639-46.
58. Asati, A.; Santra, S.; Kaittanis, C.; Perez, J. M. Surface-charge-dependent cell localization and cytotoxicity of cerium oxide nanoparticles. *ACS Nano* **2010,** *4* (9), 5321-5331.
59. Bakhti, M.; Snaidero, N.; Schneider, D.; Aggarwal, S.; Möbius, W.; Janshoff, A.; Eckhardt, M.; Nave, K.-A.; Simons, M. Loss of electrostatic cell-surface repulsion mediates myelin membrane adhesion and compaction in the central nervous system. *Proc. Natl. Acad. Sci. USA* **2013,** *110* (8), 3143-3148.
60. Wei, C.; Bard, A. J.; Feldberg, S. W. Current Rectification at Quartz Nanopipet Electrodes. *Anal. Chem.* **1997,** *69* (22), 4627-4633.
61. White, H. S.; Bund, A. Ion Current Rectification at Nanopores in Glass Membranes. *Langmuir* **2008,** *24* (5), 2212-2218.
62. Novak, P.; Shevchuk, A.; Ruenraroengsak, P.; Miragoli, M.; Thorley, A. J.; Klenerman, D.; Lab, M. J.; Tetley, T. D.; Gorelik, J.; Korchev, Y. E. Imaging single nanoparticle interactions with human lung cells using fast ion conductance microscopy. *Nano Lett.* **2014,** *14* (3), 1202-1207.
63. Lugstein, A.; Bertagnolli, E.; Kranz, C.; Kueng, A.; Mizaikoff, B. Integrating micro-and nanoelectrodes into atomic force microscopy cantilevers using focused ion beam techniques. *Appl. Phys. Lett.* **2002,** *81* (2), 349-351.
64. Şen, M.; Takahashi, Y.; Matsumae, Y.; Horiguchi, Y.; Kumatani, A.; Ino, K.; Shiku, H.; Matsue, T. Improving the Electrochemical Imaging Sensitivity of Scanning Electrochemical Microscopy-Scanning Ion Conductance Microscopy by Using Electrochemical Pt Deposition. *Anal. Chem.* **2015,** *87* (6), 3484-3489.
65. Actis, P.; Tokar, S.; Clausmeyer, J.; Babakinejad, B.; Mikhaleva, S.; Cornut, R.; Takahashi, Y.; López Córdoba, A.; Novak, P.; Shevchuck, A. I. Electrochemical nanoprobes for single-cell analysis. *ACS Nano* **2014,** *8* (1), 875-884.

66. O'Connell, M. A.; Lewis, J. R.; Wain, A. J. Electrochemical imaging of hydrogen peroxide generation at individual gold nanoparticles. *Chem. Commun.* **2015,** *51* (51), 10314-10317.
67. Actis, P.; Maalouf, M. M.; Kim, H. J.; Lohith, A.; Vilozny, B.; Seger, R. A.; Pourmand, N. Compartmental genomics in living cells revealed by single-cell nanobiopsy. *ACS Nano* **2013,** *8* (1), 546-553.
68. Zhang, Y.; Clausmeyer, J.; Babakinejad, B.; López Córdoba, A.; Ali, T.; Shevchuk, A.; Takahashi, Y.; Novak, P.; Edwards, C.; Lab, M. Spearhead Nanometric Field-Effect Transistor Sensors for Single-Cell Analysis. *ACS Nano* **2016,** *10* (3), 3214-3221.
69. Amemiya, S.; Bard, A. J.; Fan, F.-R. F.; Mirkin, M. V.; Unwin, P. R. Scanning electrochemical microscopy. *Annu. Rev. Anal. Chem.* **2008,** *1*, 95-131.
70. Chen, R.; Nioradze, N.; Santhosh, P.; Li, Z.; Surwade, S. P.; Shenoy, G. J.; Parobek, D. G.; Kim, M. A.; Liu, H.; Amemiya, S. Ultrafast Electron Transfer Kinetics of Graphene Grown by Chemical Vapor Deposition. *Angewandte Chemie* **2015,** *127* (50), 15349-15352.
71. Tan, S.-y.; Zhang, J.; Bond, A. M.; Macpherson, J. V.; Unwin, P. R. Impact of Adsorption on Scanning Electrochemical Microscopy Voltammetry and Implications for Nanogap Measurements. *Anal. Chem.* **2016,** *88* (6), 3272-3280.
72. Sun, T.; Yu, Y.; Zacher, B. J.; Mirkin, M. V. Scanning Electrochemical Microscopy of Individual Catalytic Nanoparticles. *Angew. Chem. Int. Edit.* **2014,** *53* (51), 14120-14123.
73. Lai, S. C. S.; Dudin, P. V.; Macpherson, J. V.; Unwin, P. R. Visualizing Zeptomole (Electro)Catalysis at Single Nanoparticles within an Ensemble. *J. Am. Chem. Soc.* **2011,** *133* (28), 10744-10747.
74. Güell, A. G.; Meadows, K. E.; Dudin, P. V.; Ebejer, N.; Macpherson, J. V.; Unwin, P. R. Mapping Nanoscale Electrochemistry of Individual Single-Walled Carbon Nanotubes. *Nano Lett.* **2014,** *14* (1), 220-224.
75. Byers, J. C.; Güell, A. G.; Unwin, P. R. Nanoscale Electrocatalysis: Visualizing Oxygen Reduction at Pristine, Kinked, and Oxidized Sites on Individual Carbon Nanotubes. *J. Am. Chem. Soc.* **2014,** *136* (32), 11252-11255.
76. Dasari, R.; Robinson, D. A.; Stevenson, K. J. Ultrasensitive Electroanalytical Tool for Detecting, Sizing, and Evaluating the Catalytic Activity of Platinum Nanoparticles. *J. Am. Chem. Soc.* **2013,** *135* (2), 570-573.
77. Tanner, E. E. L.; Batchelor-McAuley, C.; Compton, R. G. Single Nanoparticle Detection in Ionic Liquids. *J. Phys. Chem. C* **2016,** *120* (3), 1959-1965.
78. Castañeda, A. D.; Alligrant, T. M.; Loussaert, J. A.; Crooks, R. M. Electrocatalytic Amplification of Nanoparticle Collisions at Electrodes Modified with Polyelectrolyte Multilayer Films. *Langmuir* **2015,** *31* (2), 876-885.
79. Kang, M.; Perry, D.; Kim, Y.-R.; Colburn, A. W.; Lazenby, R. A.; Unwin, P. R. Time-Resolved Detection and Analysis of Single Nanoparticle Electrocatalytic Impacts. *J. Am. Chem. Soc.* **2015,** *137* (34), 10902-10905.
80. Chen, C.-H.; Ravenhill, E. R.; Momotenko, D.; Kim, Y.-R.; Lai, S. C.; Unwin, P. R. Impact of Surface Chemistry on Nanoparticle–Electrode Interactions in the Electrochemical Detection of Nanoparticle Collisions. *Langmuir* **2015,** *31* (43), 11932-11942.
81. O'Connell, M. A.; Snowden, M. E.; McKelvey, K.; Gayet, F.; Shirley, I.; Haddleton, D. M.; Unwin, P. R. Positionable vertical microfluidic cell based on electromigration in a theta pipet. *Langmuir* **2014,** *30* (33), 10011-10018.

82. Bayley, H.; Martin, C. R. Resistive-pulse sensing from microbes to molecules. *Chem. Rev.* **2000,** *100* (7), 2575-2594.
83. Lemay, S. G.; Kang, S.; Mathwig, K.; Singh, P. S. Single-molecule electrochemistry: present status and outlook. *Acc. Chem. Res.* **2012,** *46* (2), 369-377.
84. Howse, J. R.; Jones, R. A. L.; Ryan, A. J.; Gough, T.; Vafabakhsh, R.; Golestanian, R. Self-Motile Colloidal Particles: From Directed Propulsion to Random Walk. *Phys. Rev. Lett.* **2007,** *99* (4), 048102.
85. Xiao, X.; Bard, A. J. Observing Single Nanoparticle Collisions at an Ultramicroelectrode by Electrocatalytic Amplification. *J. Am. Chem. Soc.* **2007,** *129* (31), 9610-9612.
86. Kleijn, S. E. F.; Lai, S. C. S.; Miller, T. S.; Yanson, A. I.; Koper, M. T. M.; Unwin, P. R. Landing and Catalytic Characterization of Individual Nanoparticles on Electrode Surfaces. *J. Am. Chem. Soc.* **2012,** *134* (45), 18558-18561.
87. Sekretaryova, A. N.; Vagin, M. Y.; Turner, A. P. F.; Eriksson, M. Electrocatalytic Currents from Single Enzyme Molecules. *J. Am. Chem. Soc.* **2016,** *138* (8), 2504-2507.
88. Hoeben, F. J. M.; Meijer, F. S.; Dekker, C.; Albracht, S. P. J.; Heering, H. A.; Lemay, S. G. Toward Single-Enzyme Molecule Electrochemistry: [NiFe]-Hydrogenase Protein Film Voltammetry at Nanoelectrodes. *ACS Nano* **2008,** *2* (12), 2497-2504.
89. Olsen, T. J.; Choi, Y.; Sims, P. C.; Gul, O. T.; Corso, B. L.; Dong, C.; Brown, W. A.; Collins, P. G.; Weiss, G. A. Electronic Measurements of Single-Molecule Processing by DNA Polymerase I (Klenow Fragment). *J. Am. Chem. Soc.* **2013,** *135* (21), 7855-7860.
90. Penzo, E.; Palma, M.; Chenet, D. A.; Ao, G.; Zheng, M.; Hone, J. C.; Wind, S. J. Directed Assembly of Single Wall Carbon Nanotube Field Effect Transistors. *ACS Nano* **2016,** *10* (2), 2975-2981.
91. Bard, A. J.; Fan, F.-R. F. Electrochemical Detection of Single Molecules. *Acc. Chem. Res.* **1996,** *29* (12), 572-578.

AUTHOR INFORMATION

Corresponding Author

*P.R.Unwin@warwick.ac.uk

ACKNOWLEDGMENT

This work was supported by the European Research Council grants (ProjectRC-2009 AdG 247143-QUANTIF, M.K.) and Marie Curie Intra-European Fellowship (26158 FUNICIS, D.M.), as well as the EPSRC (Grant Number EP/F500378/1) through the MOAC DTC (A.P. and D.P.).

The authors also acknowledge Dr. Alex Colburn for the custom-built electronic equipment.

FIGURES

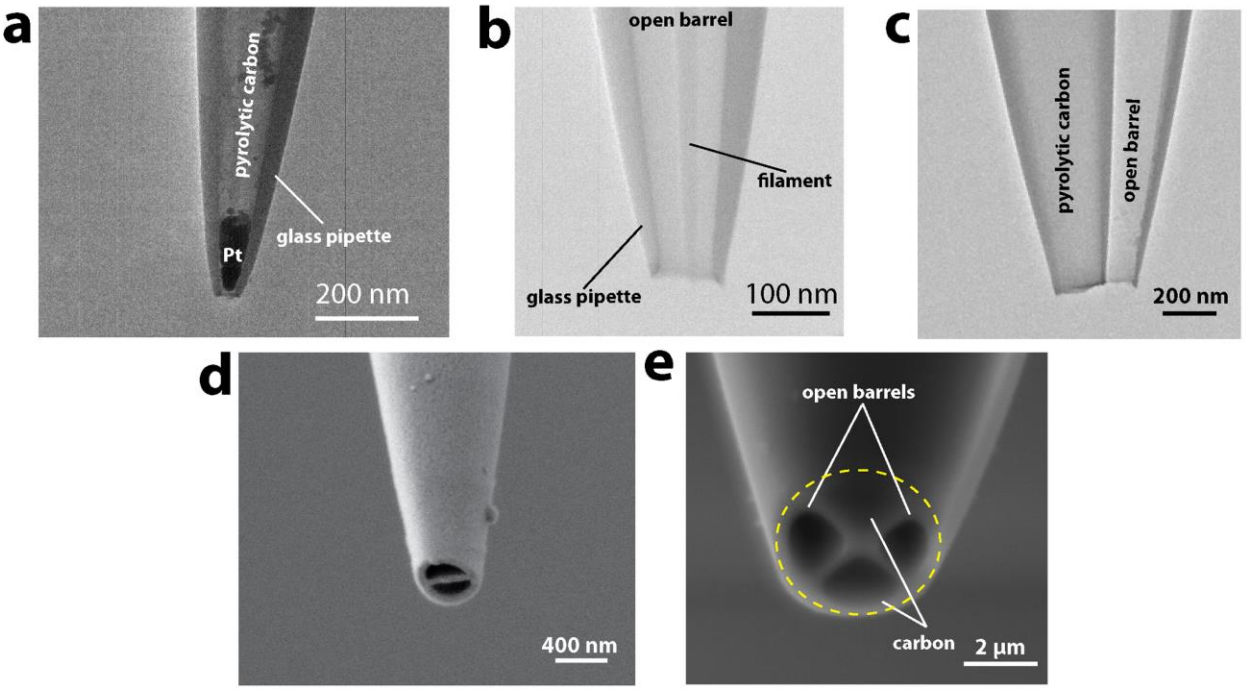

Figure 1. Electron microscopy images (transmission electron microscopy, a-c; scanning electron microscopy in d, e) of different types of nanopipette probes for electrochemical imaging. a) An amperometric SECM probe with the cavity in a carbon layer at the tip filled with electrodeposited Pt, b) an open nanopipette for SICM, c) SECM-SICM hybrid probe with pyrolytic carbon nanoelectrode and an open barrel, d) a double-barrel SECCM nanopipette (2 open channels) and e) a quad-barrel probe, (two open barrels and two channels with deposited pyrolytic carbon). Part e adapted from reference 15.

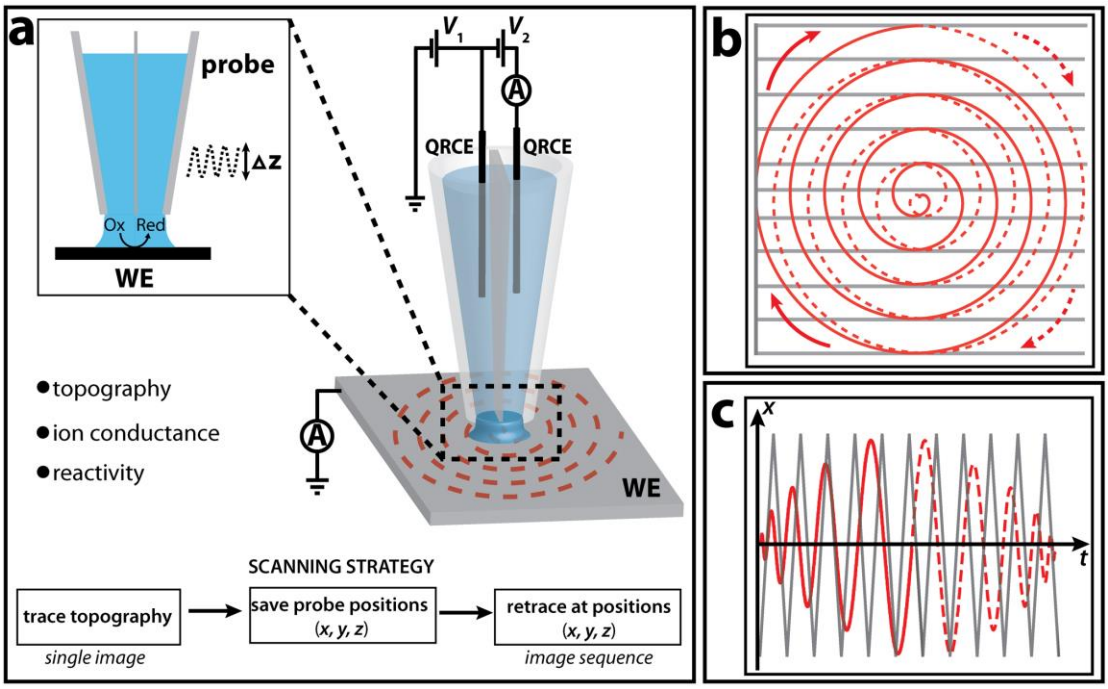

Figure 2. High-speed electrochemical imaging platform based on an SECCM setup. a) Schematic illustration of the SECCM working principle. A double-barrel nanopipette probe is equipped with two quasi-reference counter electrodes (QRCEs) and filled with electrolyte solution. A constant bias value V_2 induces a conductance current between the pipette barrels, while a variable V_1 is used to control the working electrode (substrate) potential. Vertical oscillation of the probe (Δz) gives rise to alternating current (AC) ion current components, used for positional feedback during scanning. The probe trajectory (red dashed line) illustrates the spiral scan pattern. b) Comparison between the Archimedes spiral scan (red solid and dashed lines for forward and reverse scans, respectively) and classical raster-scan pattern (gray lines) trajectories. The arrows indicate probe translation direction. c) Corresponding projections of the spiral and raster scans on the *x*-positioning axis. Taken from reference 36.

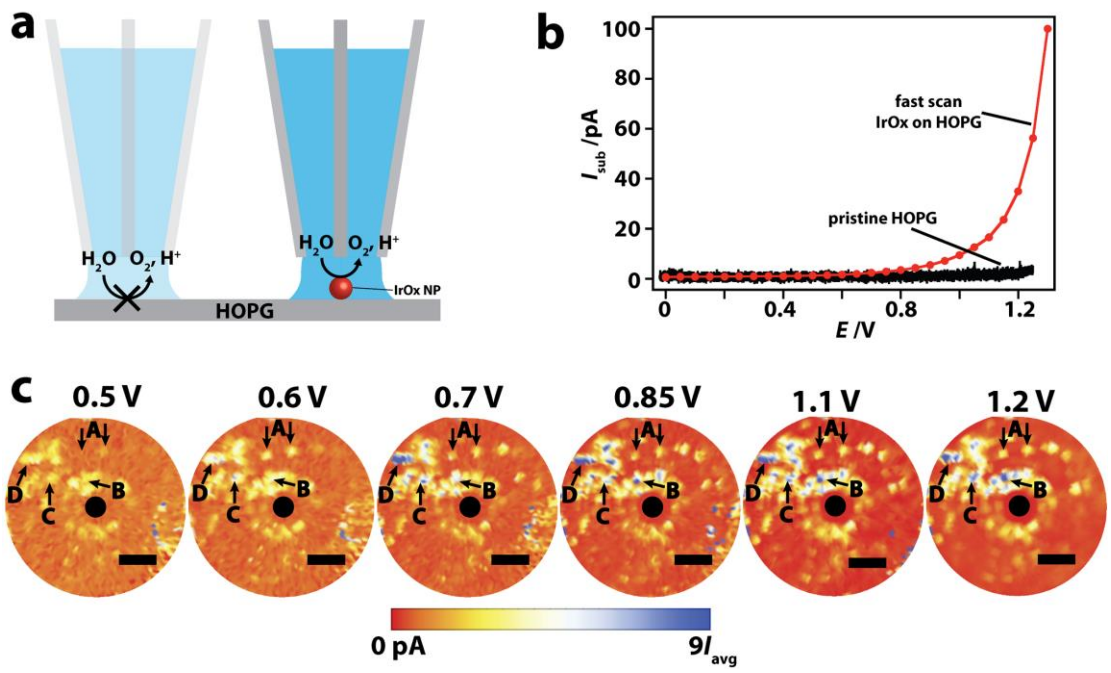

Figure 3. Imaging of electrocatalytic activity of IrO_x nanoparticles deposited on HOPG substrate for water splitting. For the potential range of interest, the electrochemical reaction essentially only occurs when the SECCM meniscus cell is in contact with a particle (a) as evidenced by linear sweep voltammograms (b), recorded at a fixed spot on a pristine HOPG (black line) and calculated from the average current values over individual frames during high-speed imaging (red line). c) A few image frames (6 forward scans out of total 30 images recorded every 12.9 s) depicting the evolution of catalytic activity of different particles (marked as "A", "B", "C" and "D") dependent on the substrate potential. The color bar is progressive with a minimum value 0 pA and maximum value that is a factor of 9 times the average substrate current, I_{avg}, at a particular potential. Scale bar 5 μm. Adapted from reference 36.

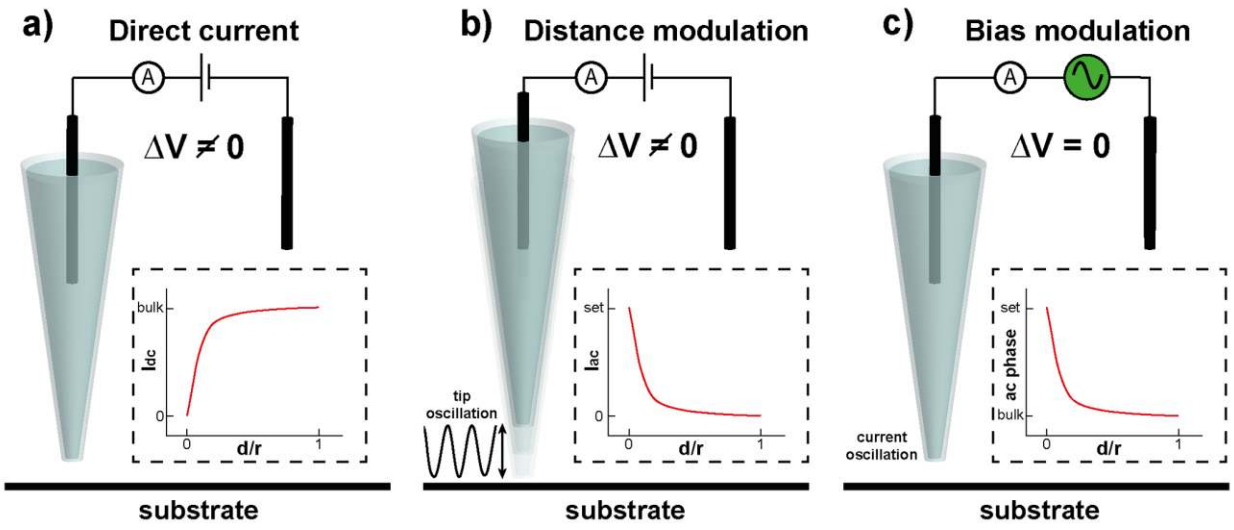

Figure 4. Comparison between different modes of SICM feedback. a) Direct current mode in which the surface is detected via a drop in ionic current. b) Distance modulation mode, with probe oscillating in vertical direction to produce an AC signal at low tip-substrate separation and (c) bias modulation mode, based on application of sinusoidal bias between the two electrodes and the readout of AC phase for feedback. Illustrative approach curves are shown in the insets on the images, revealing the feedback response as a function of relative probe-to-substrate distance *d*/*r* (physical probe-substrate separation, *d*, and probe opening radius, *r*). In b and c, 'set' indicates a set-point value for a particular quantity that is used to stop the tip moving closer to the surface and can be used for feedback during imaging.

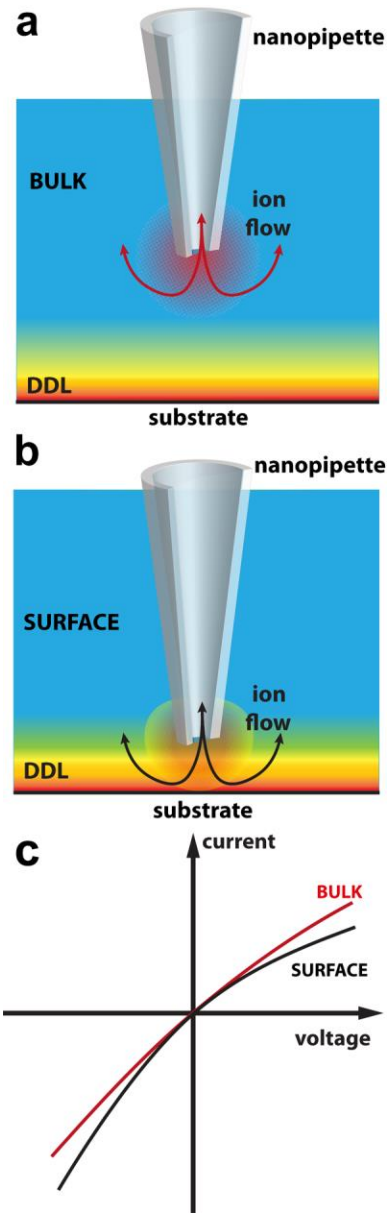

Figure 5. Schematic of the charge mapping measurement principle (not to scale). The ion flow through the pipette orifice under bias in (a) the solution bulk and (b) in the proximity of a surface, where the diffuse double layer (DDL) at the charged substrate induces rectification effects resulting in a modified mass-transport regime. Charge information is extracted from the difference between recorded voltammograms (c). The approach of the tip with zero net bias with

a BM-SICM format yields a current response that is essentially independent of charge on the substrate surface.

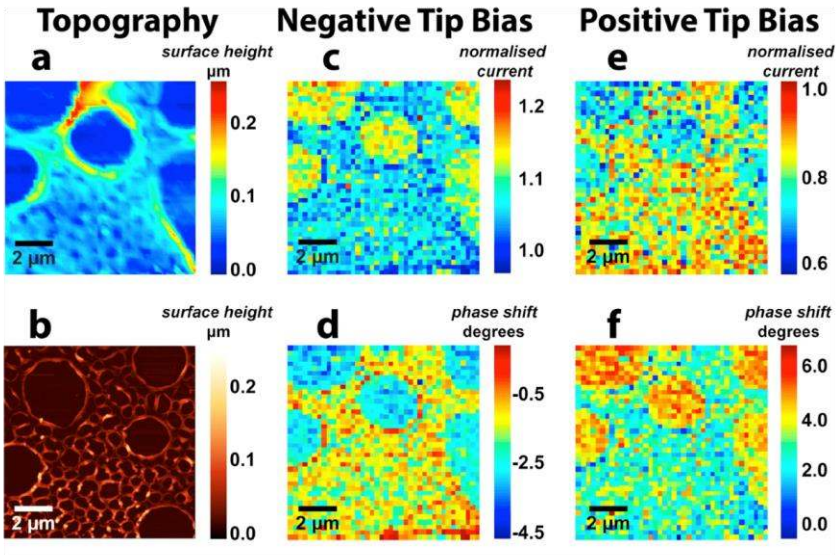

Figure 6. Simultaneous surface charge and topography maps over an imperfect polystyrene film on a glass substrate obtained with BM-SICM. (a) Topography image recorded with a ~75 nm radius nanopipette operated in a hopping mode at 0 V bias offset and (b) an AFM image of a similar area of a substrate for comparison. (c-f) Example images of the normalized DC component and AC phase shift (with the response in bulk subtracted) of the ion current at -0.3 and +0.3 V mean bias values. Adapted from reference 51.

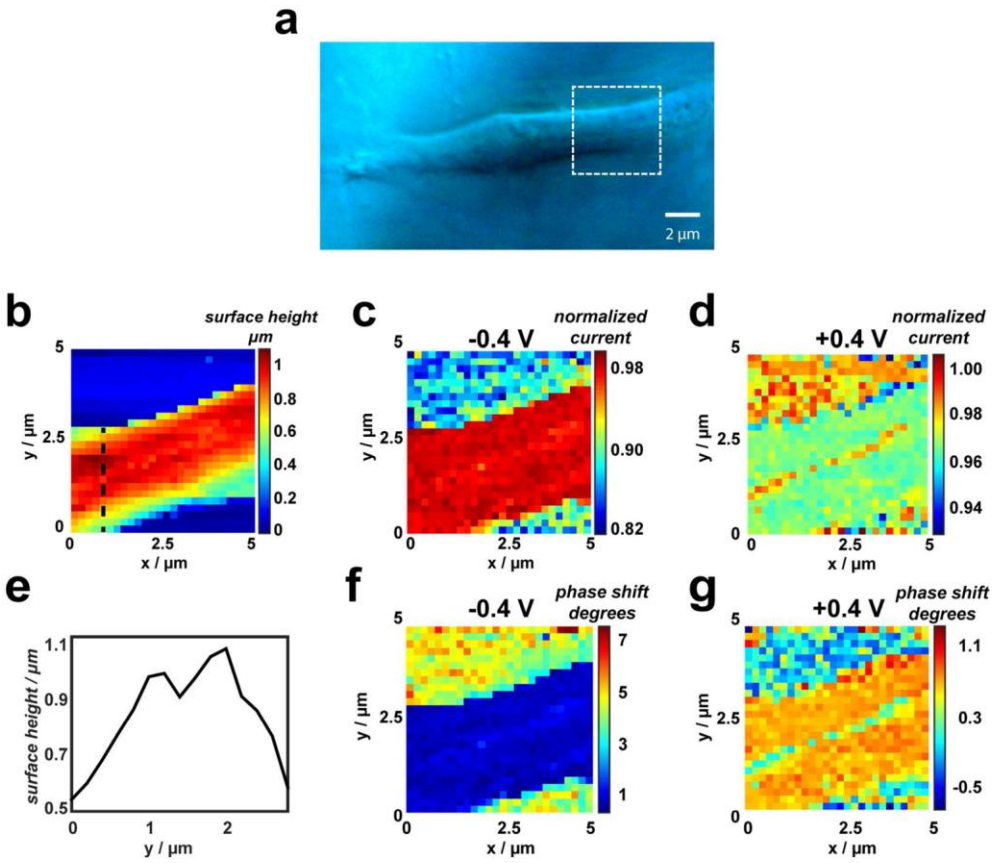

Figure 7. Simultaneous surface charge and topographical mapping of a human adipocyte cell on a collagen support using BM-SICM. (a) Optical microscope image of the spindle-shaped cell with the SICM scan region indicated by white dashed lines. (b) Topographical map, containing 26 × 26 pixels and corresponding normalized (with respect to bulk responses) DC ion current images at (c) negative (−0.4 V) and (d) positive (0.4 V) tip biases. Line profile along the black dotted line in (b) shows the change in topography across the cell and reveals a trough feature in the cell surface morphology (e). AC phase data at (f) −0.4 V and (g) 0.4 V reveal a strong contrast between the cell and collagen support. Taken from Reference 53.

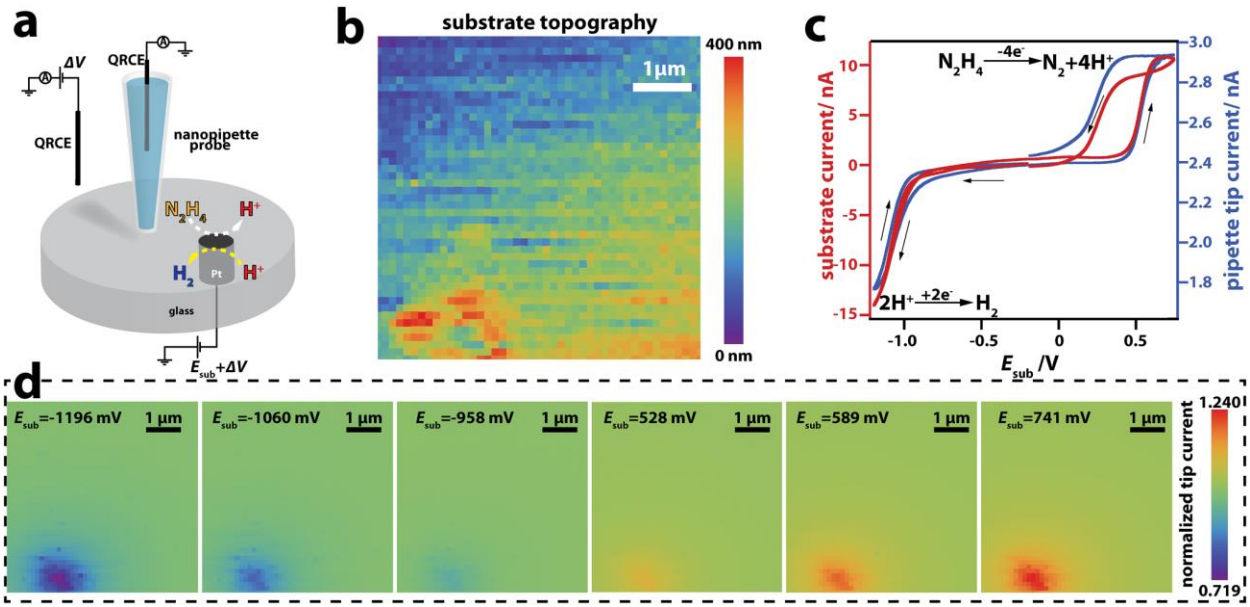

Figure 8. Simultaneous reactivity and topographical imaging with SICM. a) Schematic representation of the experimental setup. b) Topography map (45 by 45 pixels, 125 nm step size) acquired by a hopping scan. c) Recorded voltammogram at the substrate (red) and corresponding changes in the nanopipette conductance current (blue) with the nanopipette positioned above the active site on the sample. (d) Electrochemical images (6 frames) from a 380-snapshot image sequence, constructed from voltammetric data resolved at each image pixel. The nanopipette current has been normalized by the value at the point of the closest approach (at each individual pixel) with the substrate potential held at −0.2 V. Taken from reference 37.

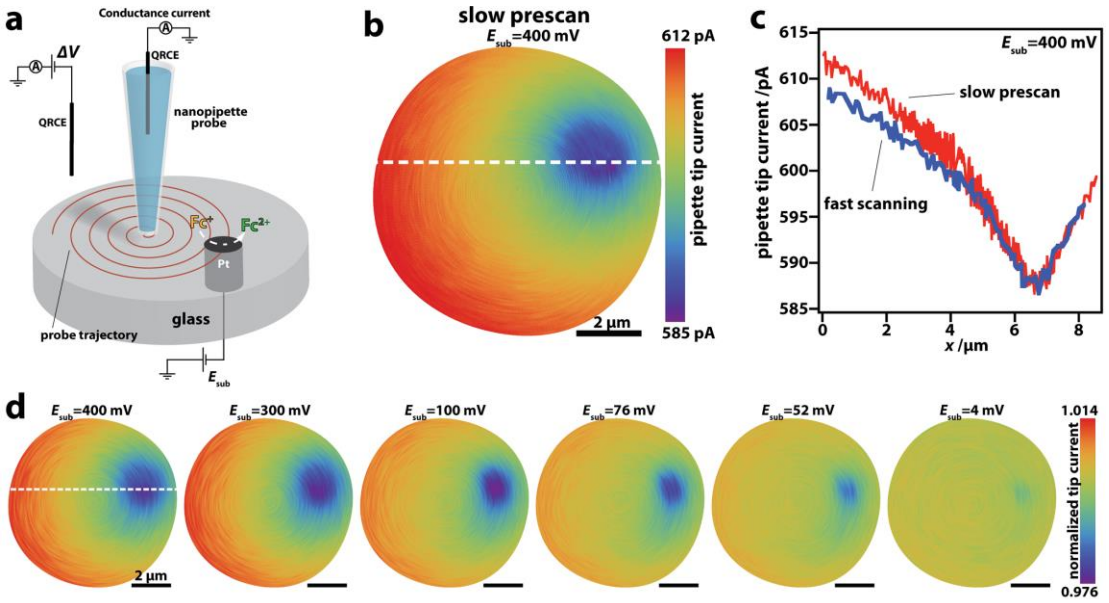

Figure 9. High-speed electrochemical imaging performed with a 95 nm radius SICM nanopipette probe (biased at -0.25 V vs. QRCE in bulk solution) over a ~430 nm radius Pt microelectrode (held at different potentials on every image frame) in electrolyte solution containing 2 mM $FcTMA^+$ and 10 mM KNO_3. a) Schematic illustration of the imaging experiment. b) Prescan image, recorded at 5.2 µm s^{-1} with the substrate biased to promote the diffusion-limited oxidation of $FcTMA^+$ to $FcTMA^{2+}$. c) Comparison between nanopipette probe current profiles acquired in the prescan and during translation at high speed (lateral probe movement ~180 µm s^{-1}) over the central part of the Pt electrode (white dashed lines on images), biased at 0.4 V (mass transport-limited $FcTMA^+$ oxidation). d) Set of normalized nanopipette conductance current images (6 out of 101 merged forward and reverse scan images), recorded at different substrate potentials during imaging at high dynamics. Scale bar 2 µm. Substrate potentials shown are vs. Ag/AgCl QRCE. Adapted from reference 37.

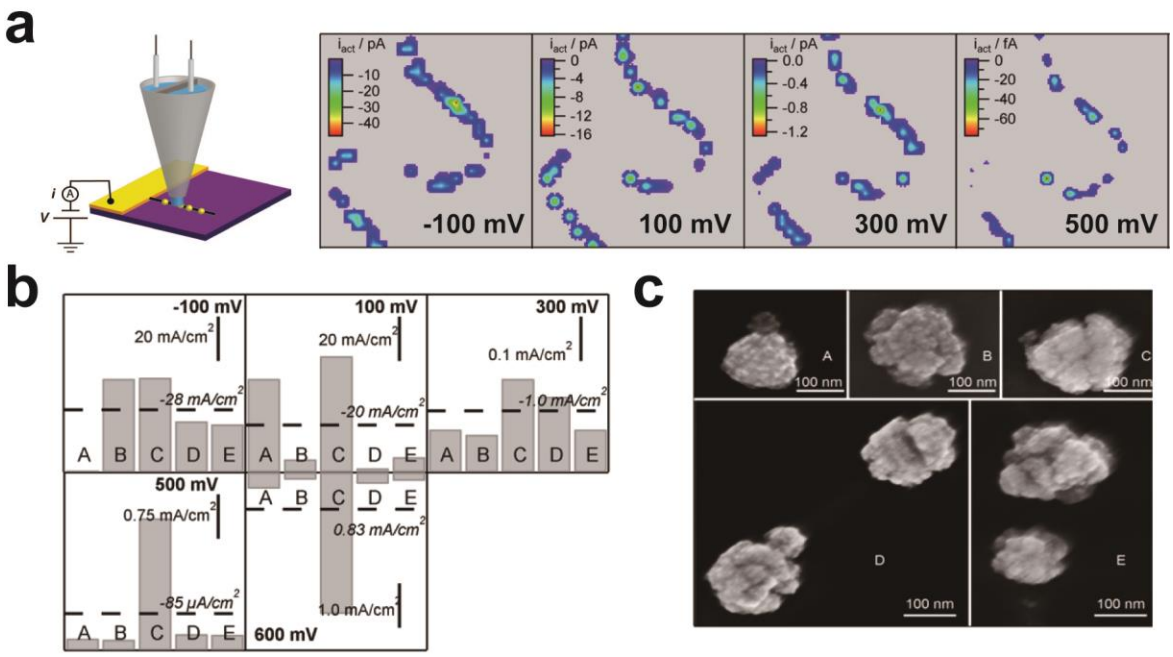

Figure 10. a) Schematic of the experimental configuration (left) and SECCM images of platinum particles deposited on a carbon nanotube showing the electrochemical response (currents) at different substrate potentials, relative to a Pd-H_2 QRCE. b) Current density plots at the various potentials (vs. Pd-H_2 QRCE) for selected particles. Current density was calculated on the basis of spherical particles using AFM particle heights (which were similar to the widths from FE-SEM). The dashed line in each plot corresponds to the average current density at that potential. Anodic currents are observed at 600 mV, with the other potentials giving cathodic currents. c) High-resolution FE-SEM images of the selected example particles. Adapted from reference 71.

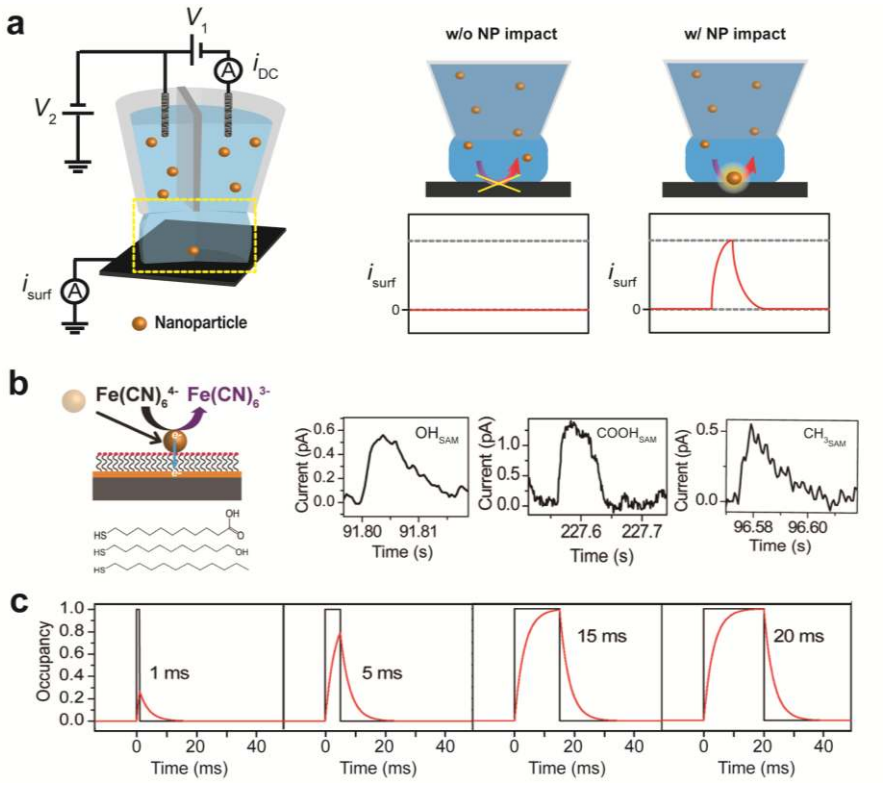

Figure 11. a) Schematic of the SECCM configuration for NP impact experiments, showing the cell set up (left), with a typical dual-barrel pipette for meniscus contact and NP delivery to a substrate electrode. i_{surf} above a background value is generated during NP impact with reaction on the substrate electrode (right). b) Principle of the electrochemical detection of single AuNP collisions on SAM-modified Au electrodes and typical responses with, −COOH, −OH, and $-CH_3$ terminated SAMs. c) Simulated current response (red lines) for a 20 ms bandwidth current follower for NP occupancy of different times (black line). Adapted from reference 78.

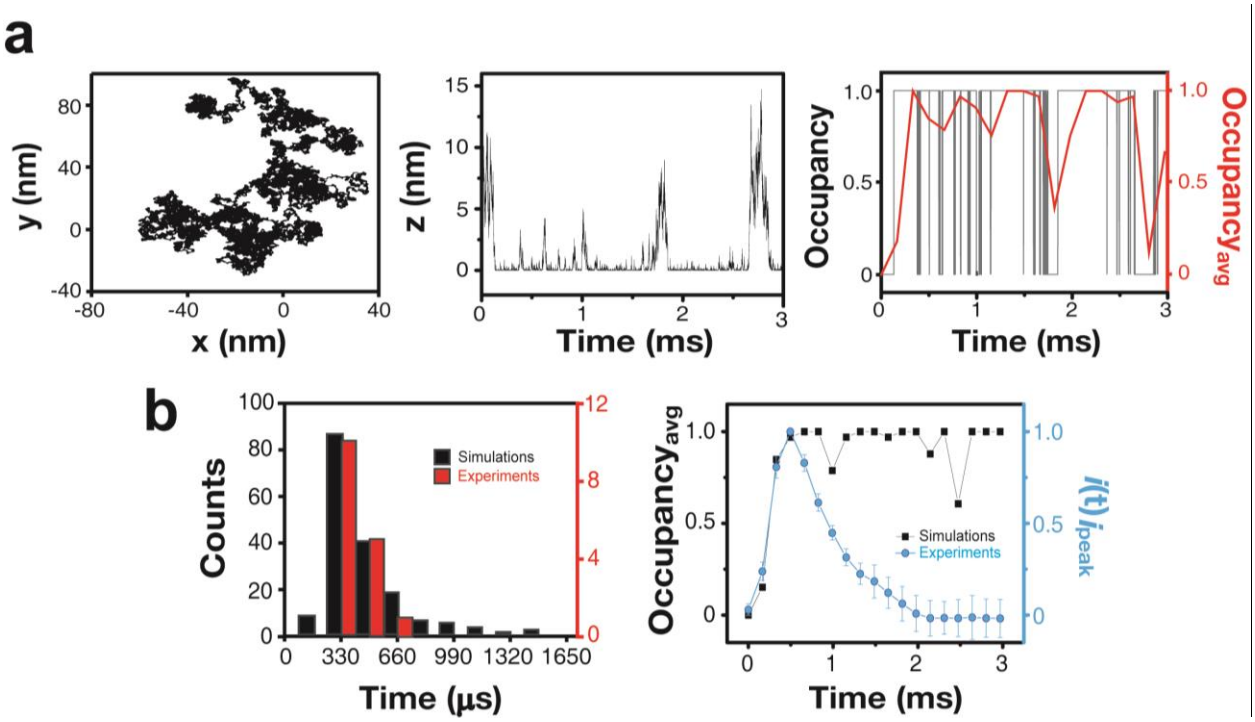

Figure 12. a) Simulated lateral (*x* and *y*) and vertical (*z* height) NP trajectory over a substrate electrode and comparison of the occupancy (black) and the average occupancy of the NP that would be seen considering the experimental conditions (red). b) Histograms of the rise time from 200 simulations (black) and 16 experimental transients (red) and an experimental *i*-*t* trace (blue line) presented alongside a simulated occupancy trace (black lines). The rise times (NP arrival) match, but experimentally the NP leaves the surface due to electrochemical propulsion (O_2 generation), which is not taken into account in the model. Adapted from reference 77.

TOC Graphic